Journal Pre-proofs

Investigation of single particle devolatilization in fluidized bed reactors by X-ray imaging techniques

Stefano Iannello, Pier Ugo Foscolo, Massimiliano Materazzi

PII: S1385-8947(21)05381-X
DOI: https://doi.org/10.1016/j.cej.2021.133807
Reference: CEJ 133807

To appear in: *Chemical Engineering Journal*

Received Date: 6 October 2021
Revised Date: 18 November 2021
Accepted Date: 20 November 2021

Please cite this article as: S. Iannello, P. Ugo Foscolo, M. Materazzi, Investigation of single particle devolatilization in fluidized bed reactors by X-ray imaging techniques, *Chemical Engineering Journal* (2021), doi: https://doi.org/10.1016/j.cej.2021.133807

Investigation of single particle devolatilization in fluidized bed reactors by X-ray imaging techniques

Stefano Iannello[a], Pier Ugo Foscolo[b], Massimiliano Materazzi[a,*]

[a] Department of Chemical Engineering, University College London, London WC1E 7JE, UK

[b] Department of Industrial Engineering and Information and Economy, Monteluco di Roio, 67100 L'Aquila, Italy

[*] Corresponding author.

E-mail address: massimiliano.materazzi.09@ucl.ac.uk

Abstract

A non-intrusive X-ray imaging technique has been used to investigate the behaviour of solid feedstock particles in a lab-scale fluidized bed reactor operated at temperatures up to 650 °C. Beech wood and polypropylene particles of different sizes have been chosen to represent the main constituents of typical thermochemical processes feedstock. The experiments were conducted under either oxidizing or inert conditions. The presence of oxygen showed a strong effect on the overall devolatilization time, which was found to be in the range of 30-112 seconds and 40-174 seconds for beech wood and polypropylene, respectively. Surprisingly, the oxidizing nature of the fluidizing medium appears to have no influence on the volatiles release within the bed in form of the so-called endogenous bubbles. These volatiles bubbles are responsible for a lift force acting on the feedstock particle itself, which ultimately encourages the segregation towards the bed surface. A one-dimensional physical model has been developed to predict particle axial location over time,

taking into account both dynamic and thermal conversion behaviour of a single feedstock particle. A revised version of the model has been proposed due to new knowledge of endogenous bubbles size provided by a novel X-ray imaging approach. Results showed very accurate predictions of the 1D model for biomass particles, which segregate towards the bed surface according to the multiple bubble segregation pattern. However, the model fails in describing plastics behaviour, possibly due to different mechanisms of reactions. The observations reported in this work show the importance of investigation at single particle level and may serve to promote new methods to gain a better understanding of plastics thermal decomposition in fluidized beds, whose mechanism is still uncertain.

Keywords

Devolatilization; Fluidized bed; Thermal conversion; Endogenous bubbles; X-ray imaging

1. Introduction

Further to struggling with the effects of global warming, our society needs to face another great challenge: to develop economic and environmentally acceptable solutions for managing the ever-increasing volumes of municipal solid waste (MSW) that are generated worldwide. Although recycling clearly has a critical role to play in reducing the amount of waste, there is further opportunity and environmental benefit in recovering energy from what might previously have been seen as materials destined for landfill [1–3]. In particular, advanced thermochemical technologies, like pyrolysis or gasification, have an important role to play in converting waste into clean energy or fuels, hence promoting the green energy transition [4–8]. When needed for thermochemical conversions, MSW is typically transformed to refuse derived fuel (RDF), which is the recovered non-recyclable fraction of MSW, after mechanical treatment, partial drying and removal of recyclable materials. Among all available technologies, fluidized bed reactors are the most promising ones and remain the

main focus for research and future exploitation of bioenergy systems [9], due to their favourable mixing features, good operating flexibility, and enhanced heat and mass transfer [10–13]. In addition, fluidized beds are extensively employed for both biomass and waste treatment, as they are capable to process a broad range of particle size [14]. However, there are still unsolved challenges when operating with highly volatile and heterogeneous feedstock (e.g. RDF), which are mainly related to poor mixing of solid and gas phases within the fluidized bed [15–20]. Waste feedstock is usually less dense than the bed material used for thermochemical applications, and therefore it is prone to axial segregation, tending to stratify along the bed height causing complications in the hydrodynamics of the bed. As a consequence, the whole volatile matter produced during the thermal decomposition segregates from the solid fuel and is mostly released into the freeboard of the reactor [10,21–23]. This phenomenon is even more evident for over-bed fuel feeding systems, which are the most commonly used industrially [24]. This has undesirable effects on the chemical reactions in the reactor, as the fuel does not take advantage of the bed-to-fuel transfer phenomena, which are essential for high product yields and quality [25,26]. The same issue is also experienced in other rector configurations, such as circulating fluidized beds, especially in dense regions that form in the bottom section of the riser [24]. All these aspects are integral part of the design of industrial fluidized bed units and relevant to all thermochemical conversions, since the evolution of volatiles is the first and common stage in pyrolysis, gasification and combustion operations. In particular, in presence of oxygen, the volatile matter ignites in the freeboard creating flames, leading to difficult temperature control. This problem is strictly connected to dimensioning and location of heat exchange surfaces and feeding points [24]. The establishment of flaming combustion in the freeboard also leads to the generation of undesired pollutants, such as NO_x [10,27] and SO_x [28]. Furthermore, several studies have shown that the volatiles released within the bed evolve in form of endogenous bubbles, which further enhance segregation of the feedstock [21–23,29,30]. Fiorentino et al. [23] developed a comprehensive mathematical model which takes into account the evolution of endogenous bubbles, while Solimene et al. [30] quantified this bubble induced effect through a lift force, which is proved to be effective to

build less intricate mathematical models [31,32]. In the past two decades, different non-invasive techniques have been developed to gain a deeper understanding of the interaction between fluidized bed and a relatively large freely moving particle. The most common methods are particle image velocimetry (PIV) [33,34], pressure signal analysis [22,35], radioactive particle tracking (RPT) [36–39], magnetic particle tracking (MPT) [15,32,40,41] and Lagrangian sensor system [42]. Most of these studies were carried out at ambient conditions using sensors or tracers to mimic the behaviour of a moving feedstock particle within the fluidized bed or investigating the hydrodynamic behaviour of the bed itself. On the other hand, the methodology developed by Bruni et al. [21] is capable to provide an online visualization of flow patterns of solids and gas phases within a bed at high temperatures with high precision. The authors used the X-ray imaging technique to investigate the axial segregation of a biomass particle during devolatilization and observed for the first time the generation of endogenous bubbles by direct visualization in a 3-dimensional bed operated at minimum fluidization condition. The advantage of this technique lies in the possibility to provide a quantitative assessment of the volatiles effect on the particle during real devolatilization conditions.

From the available literature, it is clear that the single particle approach has the advantage to provide a deeper insight regarding the behaviour of solid feedstock during thermochemical conversions in fluidized bed reactors. At present, however, most of the available studies focus on biomass particles and there is still scarce knowledge about waste feedstock of different kinds, such as mixed plastics and RDF.

The aim of this work is to provide a better understanding of the devolatilization behaviour and bed-fuel interaction in real fluidized bed reactors. This is done by investigating the main cellulosic and non-cellulosic components of RDF, separately. Beech wood and polypropylene particles were chosen to simulate the biomass and plastic fraction of waste, respectively [43]. In particular, polypropylene was chosen because of its availability and ease of sample preparation. Moreover, it represents one of the major non-recyclable constituents in solid waste [44]. This approach of separating biomass and plastic allows to avoid complications that would arise by assessing the

devolatilization behaviour of waste feedstock as a whole, because of its highly heterogeneous nature. The experiments were conducted in a fluidized bed operated at different temperatures ranging from 500 to 650 °C, which fall in the typical range of pyrolysis conditions [45]. A single particle of each material investigated was fed to the bottom of the fluidized bed by means of a purposely designed piston feeder. Minimum fluidization condition was used in order to obtain both qualitative and quantitative assessment of the volatile matter release by means of the X-ray imaging technique, and under either inert (pyrolysis) or oxidizing (gasification/combustion) condition. A comprehensive one-dimensional mathematical model was developed and used to validate experimental results, taking into account both kinetic of devolatilization and motion of the feedstock particle. Kinetic information was obtained by means of a gas analyser specifically assembled to match the strict requirements of accuracy and precision that should be considered to investigate the devolatilization of relatively small particles at high temperatures. The imaging approach used in this work provides new knowledge regarding the release of volatile matter within the fluidized bed under real thermal conversion. This assisted the development of a revised version of the model with the attempt to gain a better estimate of the endogenous bubbles lift effect.

2. Materials and methods

2.1 Model description

The model is based on the thermochemical conversion mechanism for a single feedstock particle, coupled with the equation of motion in a fluidized bed reactor. The decomposition mechanism is considered according to the nature of feedstock, namely charring and non-charring material to represent biomass and plastic, respectively. In order to simplify the computational load, particle physical properties are assumed to change along the radial direction and its position along the height

of the bed. Figure 1 shows an overview of the phenomena for the most complex case of biomass devolatilization under oxidizing condition.

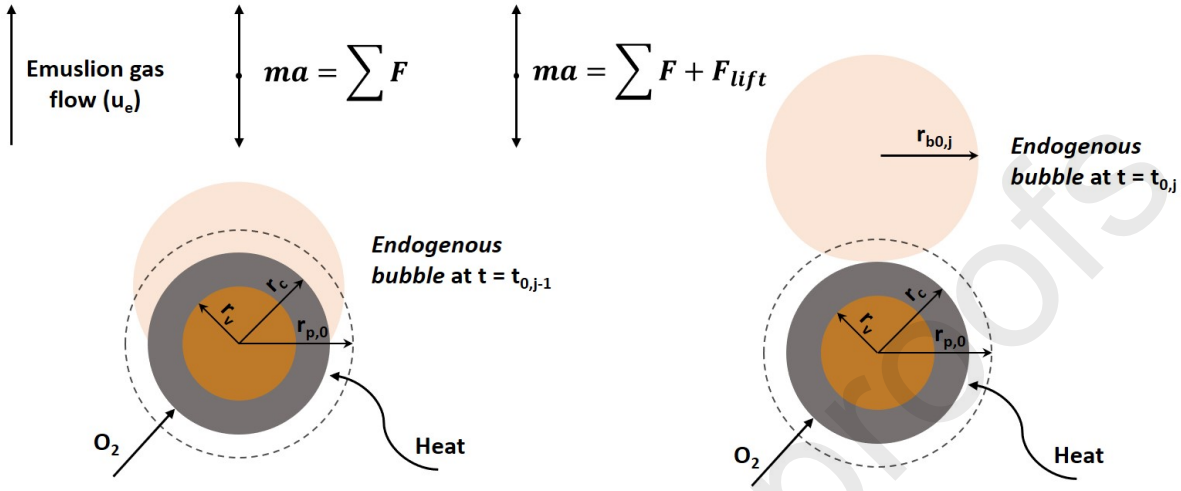

Figure 1: Schematic representation of decomposition and motion for a single biomass particle in fluidized bed under oxidizing condition.

The fluidized bed is considered as a homogeneous and continuous medium. Heating up of the particle surface occurs from the instant the particle is injected into the bed until the start of devolatilization. During this time the particle motion is not affected by the evolution of the volatiles. Since the content of moisture in the feedstock used is generally much lower than that of volatile matter [43,46–49], the drying stage has been assumed to have not a significant effect on the evolution of endogenous bubbles and change in particle density. As the surface temperature reaches the devolatilization temperature, volatile matter is released from the particle and the equation of motion is solved with a varying time step according to the time elapsed between two consecutive generated endogenous bubbles. The minimum temperature at which the devolatilization occurs has been assumed to be 390 °C [50] and 363 °C [51] for beech wood and polypropylene, respectively. These values have been used to define the onset of devolatilization, which takes place after initial heating of the particle. For the biomass particle, the char oxidation starts as soon as the first layer of carbon

142 forms on its outer surface. It is important to consider decomposition and particle motion to occur
143 simultaneously, as the change in particle properties (i.e., size and density) affects the dynamic
144 behaviour itself. Each stage of particle heating up and conversion is described in detail in the
145 following sections. Further details about the computational procedure are reported in Supplementary
146 material.
147

148 2.1.1 Heating up of the particle

149 The heating up stage for a spherical feedstock particle follows the heat equation, along with the
150 initial (IC) and boundary (BC) conditions:
151

$$\frac{\partial T}{\partial t} = \frac{\alpha}{r^2}\frac{\partial}{\partial r}\left(r^2\frac{\partial T}{\partial r}\right) \qquad (1)$$

IC $$T(t=0) = 25\ ^{\circ}C \quad , 0 \le r \le R$$

BCs $$-\lambda\frac{\partial T}{\partial r}|_{r=0} = 0 \quad , t > 0$$

$$-\lambda\frac{\partial T}{\partial r}|_{r=R} = h(T - T_{bed}) + \sigma\epsilon_{eff}(T^4 - T_{bed}^4) \quad , t > 0$$

152 During this stage all the particle properties are constant since the drying stage has been assumed
153 to have negligible effects on the evolution of endogenous bubbles and change in particle density
154 [52,53]. This is specifically true in this study due to the relatively low content of moisture in materials
155 used. The meaning of symbols is reported in the nomenclature section at the end.
156

2.1.2 Particle devolatilization

In this work, the devolatilization stage has been considered as a heat-neutral phenomenon, assuming that the exothermic and endothermic steps of thermal degradation balance each other [54,55]. This assumption is common in literature, where several authors neglected the contribution of heat of drying and devolatilization in their models [52,53].

The apparent kinetic of devolatilization for a solid feedstock particle can be described by the following pseudo-first order rate law:

$$\frac{dX}{dt} = k\,(1 - X) = A_i e^{-\frac{E_a}{RT}}(1 - X) \qquad (2)$$

where X is the solid mass conversion. The devolatilization time for a single particle is usually expressed as a function of its initial size by a power law [56,57]. In the present case, the dependence on the particle size is included in the pre-exponential factor, as suggested by Jand and Foscolo [54]:

$$A_i = A_r\left(\frac{d_{p0,r}}{d_{p0,i}}\right)^{\psi} \qquad (3)$$

where A_r and $d_{p0,r}$ are the reference pre-exponential factor and initial particle diameter, respectively. The integration of the Eqn. 2 and 3 from t = 0 to the end of devolatilization t = t_d, gives the following expression:

$$ln\, t_d = ln\,[-ln\,(1 - X_d)] - \psi\, ln\, A_r\left(\frac{d_{p0,r}}{d_{p0,i}}\right) + \frac{E_a}{RT} \qquad (4)$$

The high heat transfer coefficient of fluidized beds [37,54,58,59] ensures high heating rates. We can then assume devolatilization to occur at the constant bed temperature.

The pre-exponential factor, activation energy and parameter ψ, have been obtained experimentally and are discussed in the results section. From the rate law, the volumetric volatiles flow rate can be written as:

$$Q = \frac{m_{p0}\, w dX}{\rho_{vm}\ dt} = \frac{m_{p0}\, w}{\rho_{vm}} k e^{-k(t - t_{in})} \qquad (5)$$

where t_{in} is the induction time calculated from the heating up stage, which varies between 0.3% and 0.7% of the whole devolatilization time, according to the nature and size of the feedstock particle. Phenol [60] was chosen as ideal gaseous pseudo-component for the calculation of ρ_{vm} for beech wood particle. For the volatiles emitted from polypropylene, naphthalene [61] was assumed as lumped component, due to the near-zero concentration of oxygen in the raw polymer molecule [46,47]. In this context, knowledge about the rate of volatile production is important for the estimation of the lift force induced by the endogenous bubbles.

During this stage, the particle size decreases according to the rate law:

$$\frac{dd_v}{dt} = -\frac{k\, d_v}{3} \qquad (6)$$

2.1.3 Char burnout

The char burnout stage is considered in the case of biomass (charring material) under oxidizing conditions. Oxygen diffuses from the surrounding to the surface of char, causing particle shrinkage [58]. Therefore, the decomposition of char is assumed to be controlled by the external mass transfer of oxygen, and follows the shrinking core model:

$$\frac{dd_c}{dt} = -\frac{2\,\beta\, k_g\, M_c\, y_o\, \rho_f}{\rho_c\, M_f} \qquad (7)$$

where the subscripts *v* and *c* indicate the virgin core and char of the particle, respectively, as shown in Figure 1. The above assumption ensures that the oxygen is consumed at the boundary of the char layer and the heat of combustion is not released inside the particle.

The overall density of the particle can be calculated as a function of the varying size of virgin core and char layer by the following equation:

$$\rho_p = \frac{\rho_v d_v^3 + \rho_c d_c^3 + 6\, m_t/\pi}{d_c^3} \qquad (8)$$

where m_t is the mass of the lead tracer used to track the particle during the experiments. It is important to note that equations 7 and 8 describe the most complex case of a decomposing biomass particle under oxidizing condition. On the other hand, for the polymer particle the char layer does not form (non-charring material), and the overall particle density can be calculated as follows:

$$\rho_p = \frac{\rho_v d_v^3 + 6\, m_t/\pi}{d_v^3} \qquad (9)$$

2.1.4 Particle motion and criterion for endogenous bubbles detachment

The motion of a relatively large object immersed in a fluid can be described by the sum of the forces acting on it:

$$F_{tot} + F_m = F_g + F_b + F_d + F_{lift} \qquad (10)$$

The volatile bubbles generated during devolatilization induce a lift effect on the particle through F_{lift}. However, it is assumed that the momentum transferred to the particle takes place when the bubble is at the edge of detachment [30]. Assuming the bubbles evolution to occur with the same mechanism of bubble formation through an orifice, diameter and time for the j-th endogenous bubble at the detachment are given by the following equations [58]:

$$d_{b0,j} = 1.259 \frac{Q_j^{0.4}}{g^{0.2}} \qquad (11)$$

$$t_{0,j} = \frac{V_{b0,j}}{Q_j} + t_{0,j-1} \qquad (12)$$

where $t_{0,j-1}$ is the detachment time of the bubble j-1, which is assumed to be equal to the formation time of the bubble j. For the first iteration, $t_{0,j-1}$ is equal to the induction time t_{in}. According to this criterion, the lift force acts on the particle every time that $t = t_{0,j}$ during the devolatilization period. The approach of time discretization described above offers the advantage of reducing significantly the time of computation, although preserving the accuracy in predictions.

Table 1 and 2 show the equations and physical parameters used for the computation, respectively.

Table 1: Equations assumed for the modelling of particle decomposition and motion [24].

Name	Equation	
	Heating up of particle surface	
Effective bed emissivity	$\epsilon_{eff} = \left(\frac{1}{\epsilon_p} + \frac{1}{\epsilon_{bed}} - 1\right)^{-1}$	(13)
Bed emulsion emissivity	$\epsilon_{bed} = \epsilon_s^{0.485}$	(14)
	Particle decomposition	
Diffusivity of oxygen in nitrogen, [m^2/s] [62]	$D_{oN} = \frac{\left[10^{-3}\, T^{1.75} \left(1/M_o + 1/M_N\right)^{0.5}\right]}{P\left(v_o^{\frac{1}{3}} + v_N^{\frac{1}{3}}\right)^2}$	(15)
Particle Reynolds number at U_{mf}	$Re_{mf} = \frac{\rho_f\, U_{mf}\, d_c}{\mu_f}$	(16)
Schmidt number	$Sc = \frac{\mu_f}{\rho_f\, D_{oN}}$	(17)
Fluid density, [kg/m^3]	$\rho_f = \frac{P\, M_f}{R\, T}$	(18)

Fluid viscosity, [Pa s] [63]

$$\mu_f = \frac{C_1\, T^{C_2}}{1 + \frac{C_3}{T} + \frac{C_4}{T^2}} \tag{19}$$

Fluid molecular weight, [kg/mol]

$$M_f = y_o\, M_o + (1 - y_o)\, M_N \tag{20}$$

Sherwood number

$$Sh = \frac{k_g\, d_c}{D_{oN}} = 2\varepsilon_{mf} + 0.69\left(\frac{Re_{mf}}{\varepsilon_{mf}}\right)^{0.5} Sc^{\frac{1}{3}} \tag{21}$$

Particle motion

Overall external force on the feedstock particle, [N]

$$F_{tot} = \frac{\pi}{6}\,\rho_p\, d_c^3\, \frac{d^2 z_p}{dt^2} \tag{22}$$

Added mass force, [N]

$$F_m = \frac{\pi}{12}\,\rho_e\, d_c^3\, \frac{d^2 z_p}{dt^2} \tag{23}$$

Gravitational force, [N]

$$F_g = -\frac{\pi}{6}\,\rho_p\, d_c^3\, g \tag{24}$$

Buoyancy force, [N]

$$F_b = \frac{\pi}{6}\,\rho_e\, d_c^3\, g \tag{25}$$

Drag force, [N]

$$F_d = \frac{\pi}{8}\,\rho_e\, C_D\, d_c^2 (\, u_e - v_p)\, |\, u_e - v_p| \tag{26}$$

Lift force, [N] [30]

$$F_{lift} = 0.372\, g^{0.6}\, \rho_e\, d_v\, Q^{0.8} \tag{27}$$

Drag coefficient [32]

$$C_D = \frac{24}{Re}(1 + 0.15\, Re^{0.687}) \tag{28}$$

Particle Reynolds number

$$Re = \frac{\rho_e\, |\, u_e - v_p|\, d_c}{\mu_e} \tag{29}$$

Density of bed emulsion, [kg/m^3]

$$\rho_e = \frac{4\, m_{bed}}{\pi\, d_{bed}^2\, H_{bed}} \tag{30}$$

Interstitial velocity of emulsion gas, [m/s] [58]

$$u_e = \frac{U_{mf}}{\varepsilon_{mf}} \tag{31}$$

Bed void fraction at U_{mf}

$$\varepsilon_{mf} = 1 - \frac{\rho_e}{\rho_s} \tag{32}$$

226

Table 2: Physical parameters used for the computation.

Name	Value	Ref.
Stefan-Boltzmann constant, [W/m^2 K^4]	$\sigma = 5.67 \times 10^{-8}$	
Feedstock emissivity	$\epsilon_p = 0.8$ (BW)	[54,63]
	$\epsilon_p = 0.9$ (PP)	
Bed particle emissivity	$\epsilon_s = 0.8$	[54]
Feedstock thermal conductivity, [W/m K]	$\lambda = 0.29$ (BW)	[64,65]
	$\lambda = 0.15$ (PP)	
Heat transfer coefficient, [W/m^2 K]	$h = 335$	[54]
Pore volume per unit mass of char, [m^3/kg]	$V_{pore} = 0.23 \times 10^{-3}$	[66]
Viscosity of bed emulsion, [Pa s]	$\mu_e = 0.15$	[22]

2.2 Experimental apparatus

2.2.1 Feedstock

Beech wood and polypropylene spheres with 3 different diameters (8, 10 and 12 mm) have been chosen to resemble the biomass and synthetic polymer fraction of RDF, respectively. All the samples were half-drilled in order to insert a small tracer of lead ranging from 1.5 to 2 mm to make the particle visible upon X-ray exposure during the experiments. Figure 2 shows the particles used for the experiments. Typical physical and chemical properties of the materials investigated are listed in Table 3.

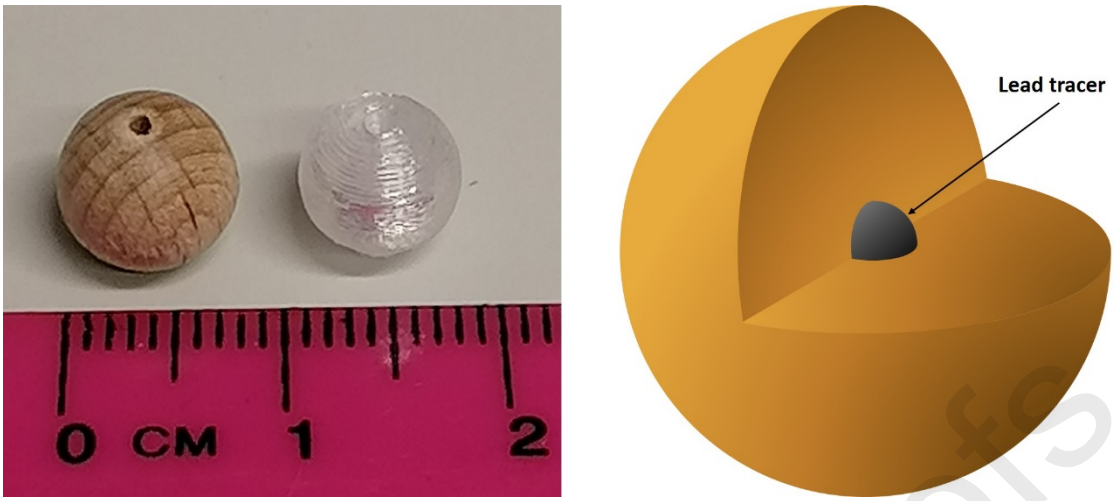

Figure 2: Particles of beech wood and polypropylene used for the experiments (left) and simple representation of the sample with a small lead tracer in its centre (right).

Table 3: Typical physical and chemical properties of beech wood and polypropylene.

	BW			**PP**	
Ref.	[43]	[48]	[49]	[46]	[47]
Ultimate analysis, (wt%)	db	daf	db	ar	daf
C	48.1	49.2	49.1	86.42	84.62
H	5.9	6.0	5.7	12.28	15.23
O	45.4	44.1	44.5	-	0
N	0.2	0.5	0.15	0.72	0.14
S	-	0.02	0.045	0.17	0.01
Proximate analysis, (wt%)	wb	db	db	db	db
Volatiles	74.8	85.3	84.3	99.3	99.79
Fixed carbon	15.7	14.3	15.2	-	0.13
Ash	0.7	0.4	0.5	0.7	0.08
Moisture	8.8	0	8.7^{ar}	-	-
Heating value db, [MJ/kg]	15.0	-	-	44.7	45.8
Physical properties (this work)					
Diameter, [mm]	8, 10, 12				
Density, [kg/m^3] (raw sample)	774 ± 0.012			697 ± 0.011	
Density, [kg/m^3] (with lead tracer)	900				

ar: as received, daf: dry ash free, db: dry basis, wb: wet basis

Beech wood particles have been acquired with an existing hole within, while polypropylene particles were designed in SolidWorks® as half-drilled spheres and 3D printed using a natural polypropylene filament and an Ultimaker 3. The diameter of the hole was between 2 mm (10 and 12

mm particles) and 1.5 mm (8 mm particle). The initial density of particle including the lead tracer was measured to be 900 kg/m^3 for both samples, which falls within typical ranges of density for pelletized RDF feedstock (665 – 1200 kg/m^3) [67–70]. The density changes with time during thermal conversion were estimated according to equations 8 and 9.

2.2.2 Fluidized bed reactor

The experimental apparatus consists of a 146 mm ID × 1000 mm high Inconel tube fitted with a stainless-steel distributor plate and is operated at atmospheric pressure and temperatures of 500, 600 and 650 °C. The temperature levels used in this work are high enough to provide devolatilization of the feedstock (above minimum devolatilization temperature mentioned above) and they fall in the typical range of pyrolysis operations [71]. The vessel was filled with a Geldart group B quartz sand (particle density 2650 kg/m^3 and average particle size 250 μm) up to a fixed bed height of 13 cm at ambient temperature. This allows sufficient volume in the freeboard to homogenize and cool down the released gas before the sampling point of the gas analyser. Either air or nitrogen were used as fluidizing media to operate under oxidizing and inert conditions, respectively. Figure 3 shows a simple scheme of the whole experimental apparatus.

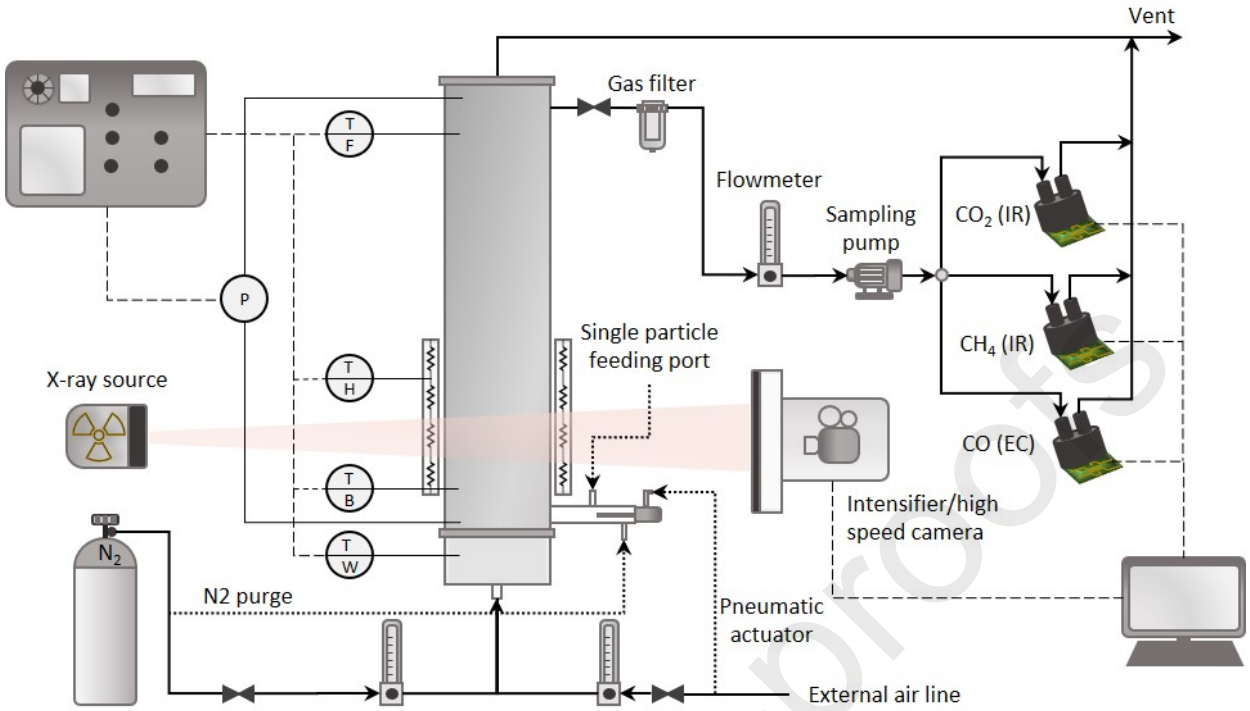

Figure 3: Experimental apparatus. F: freeboard, H: electric heater, B: fluidized bed, W: windbox.

The system is equipped with a purposely designed single fuel particle injector located at 2.5 cm above the distributor plate to simulate the under bed feeding modality of the feedstock. It consists of a 28 cm piston rod enclosed in a 50 cm stainless steel tube, which can be driven by a pneumatic actuator into the reactor. At rest, the piston is retracted to allow the placement of the feedstock particle into the tube through a threaded hole, which is then closed with a bolt to isolate the entire system from the environment. Subsequently, nitrogen is fed through the tube to remove residual air and prevent heating and reaction before the particle injection. A single particle of either beech wood or polypropylene was fed into the reactor during each experimental run. The bed was operated at minimum fluidization for all the experiments to enable observation of volatiles without possibilities of confusion arising from the fluidizing gas bubbles. The evolution of gas from a relatively small particle in fluidized beds is a fast phenomenon, due to the high heating rates the feedstock experiences in this type of reactors. For this reason, specific gas sensors have been chosen according to their high sensitivity and low response time in order to minimize the error associated with the estimations of

279 devolatilization. CO_2 measurements were carried out with a GSS SprintIR-WF-20®, while CO and
280 CH_4, including also other hydrocarbon species, were collected with CO2METER® sensors. The gas
281 detectors were placed in parallel to allow each gas species to be measured simultaneously, as shown
282 in Figure 3. The sampling gas flow rate was set at 1 lpm. The measured concentrations have been
283 corrected taking into account the dispersion phenomena along the reactor and sampling line to the
284 measurement point. An extensive explanation of the determination of true gas concentrations in
285 similar systems is reported in literature [72–75]. Figure 4 shows a typical trend of measured volatiles
286 evolution as a function of time, raw data along with the true profile obtained after correction. In
287 Supplementary material, concentration vs time in the reactor freeboard is reported for each measured
288 volatile species.
289

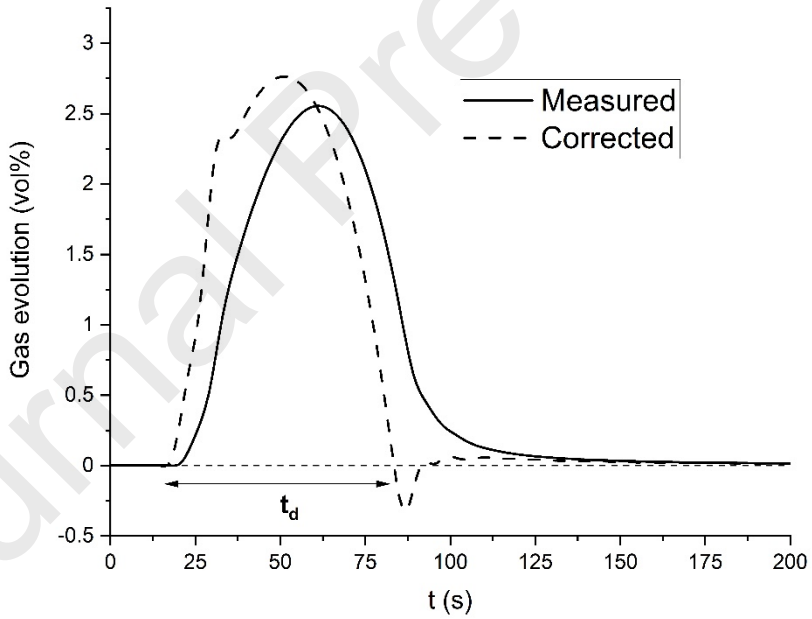

290
291 Figure 4: Typical gas evolution profile vs time from devolatilization of a single particle.

292 From the collected data it was possible to determine the kinetic of devolatilization, as discussed in
293 the results section.
294

2.2.3 X-ray facility and imaging techniques

The non-invasive X-ray technique provides frame-by-frame imaging with extremely high time resolution (36 frames per second). The system was operated for cine exposure recording (cineradiography). The collected raw images need to be post-processed in order to perform any quantitative analysis. For this purpose, different algorithms for image analysis were developed and implemented in MATLAB® [76]. The main steps to be considered are:

- Correction of pincushion distortion due to the intrinsic curvature of the image intensifier and diverging conical shape of the X-ray beam, as shown in Figure 3. The visual effect that these features generate is a distortion of the image boundaries, which appear to be bowed inwards towards the centre. The pincushion distortion can be reduced by increasing the source-to-intensifier distance (SID) and decreasing the object-to-intensifier distance (OID). In this case, the object is the fluidized bed reactor. The optimal values of SID and OID used in this work to minimize this effect are 99 cm and 26 cm, respectively.
- Determination of the magnification factor that provides the conversion from pixels to SI units. This is achieved by placing a square lead marker of given dimensions (1 cm × 1 cm) on the external surface of the insulation of the reactor at a distance from the distributor greater than the height of the expanded bed, so that its presence in the images does not disrupt subsequent measurements and particle tracking.
- Selection of a region of interest (ROI) for each image in order to remove all the regions that are not important for any subsequent analysis, such as the area of the freeboard and lead marker.
- Application of filtering functions to improve the contrast between lead tracer in the feedstock particle and background (bed emulsion). This step is crucial to automate the process of particle tracking.

- Particle tracking based on the Kalman filter algorithm to determine the location of the feedstock particle within the bed.

The height of the expanded bed was estimated by different frames recorded in time series. From the measured values it is possible to calculate both density and void fraction of the bed using equations 30 and 32 reported in Table 1. Moreover, the images acquired were also used for the determination of the endogenous bubbles size. The high difference in attenuation of X-ray beams between solid and gas phases allows to visualize the volatiles bubbles and distinguish them from the bed material very clearly. Each released bubble was assumed to be spherical and the equivalent circle in each frame to represent the cross-sectional area of the bubble itself. Observation of endogenous bubble is shown in Figure 5. This information has been proved extremely useful to obtain a better quantitative assessment of the lift effect induced by the volatiles on the particle during devolatilization.

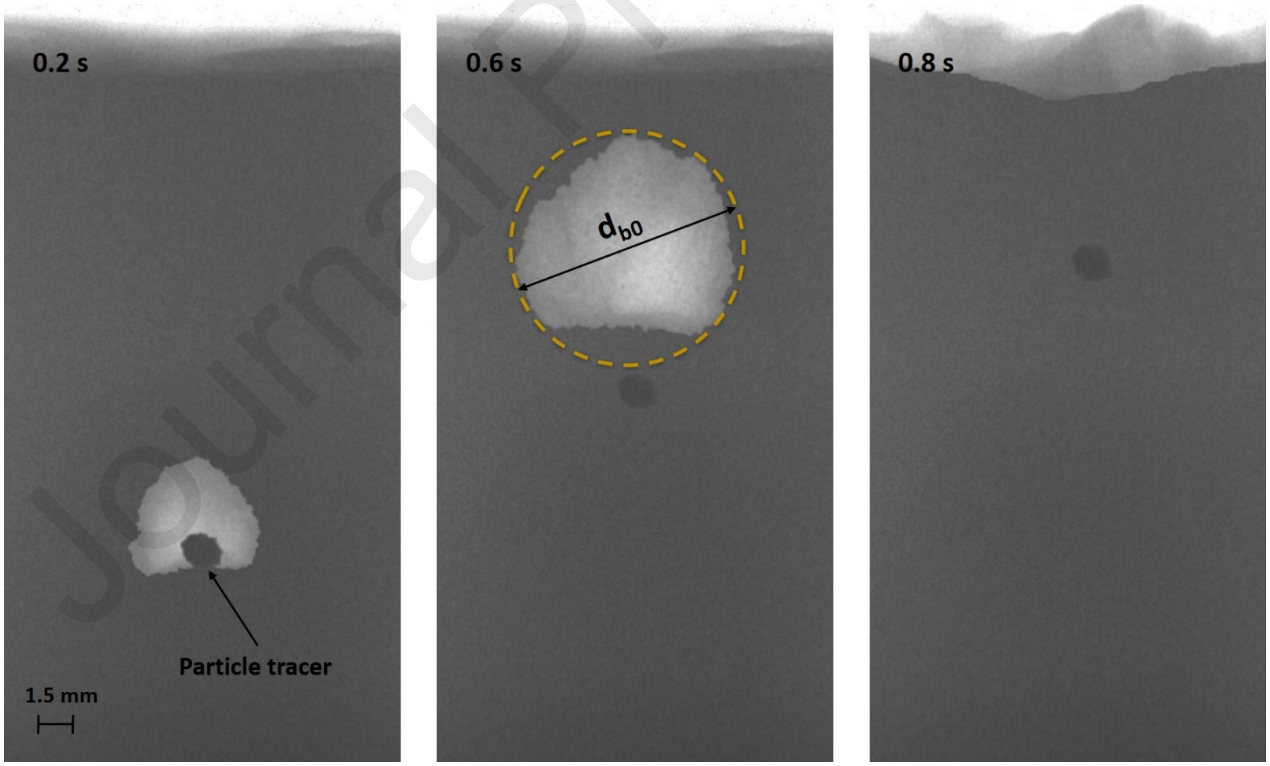

Figure 5: From left to right: formation, detachment and eruption of an endogenous bubble from a biomass particle (8 mm diameter) at 650 °C in a selected ROI.

Furthermore, from the images acquired it was possible to determine the frequency of endogenous bubbles formation. Comparison between observations and model prediction is discussed in the next section.

3. Results and discussion

3.1 Kinetic of devolatilization

The kinetic parameters have been found following the fitting procedure reported by Jand and Foscolo [54]. The smallest particle diameter was chosen as a reference ($d_{0i} = d_{0r} = 8$ mm) for the determination of A_r and apparent activation E_a with a first linear regression on the experimental data. The devolatilization time data for the biggest particle (12 mm) was used to evaluate the exponent ψ with a second fitting step. The final mass conversion X_d has been assumed according to the volatile matter content of the material. Typical values from proximate analysis are 0.85 [48,49] and 0.99 [46,47] (w/w dry basis) for beech wood and polypropylene, respectively.

Figure 6 shows experimental and predicted devolatilization time under both oxidizing and reducing conditions; the kinetic parameters are listed in Table 4. As mentioned above, further details about the measured concentration profiles of volatile species are reported in Supplementary material.

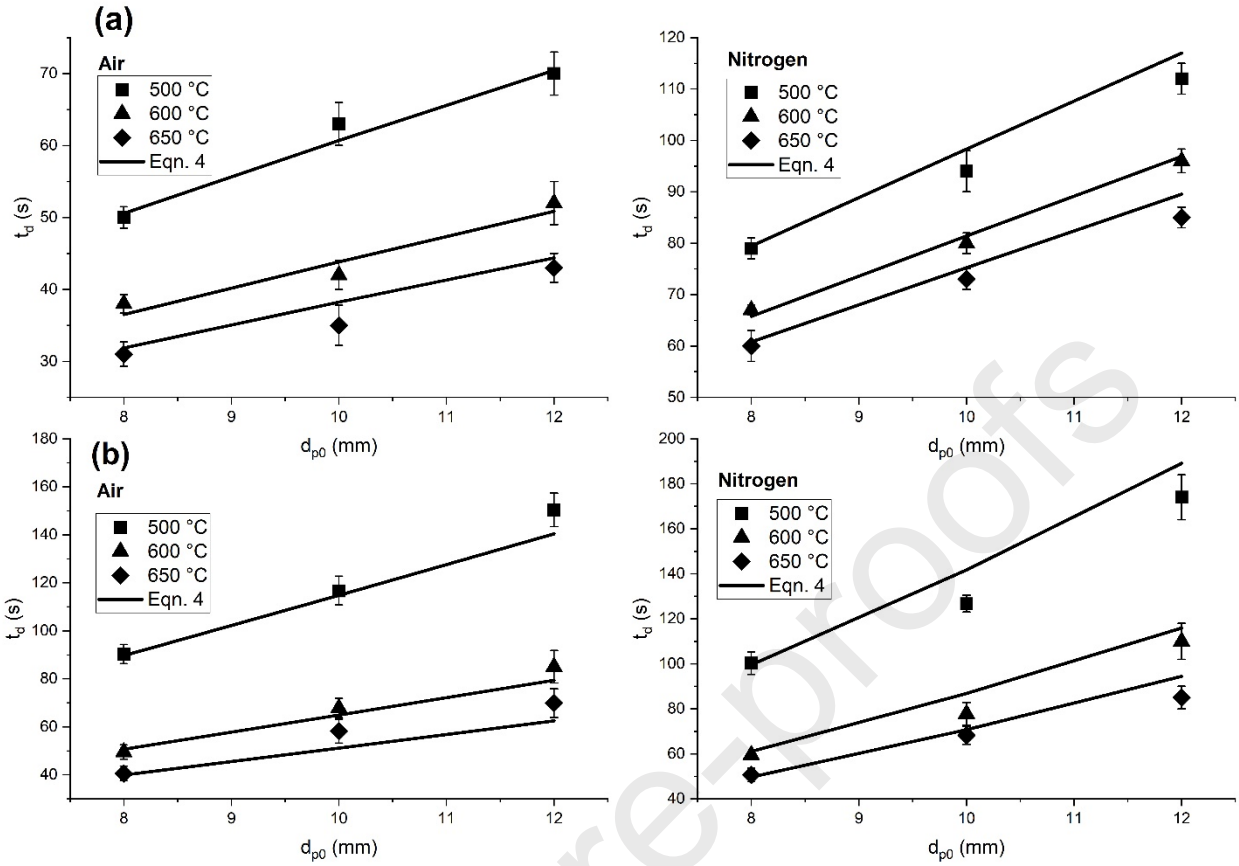

Figure 6: Experimental and calculated devolatilization time for beech wood (a) and polypropylene (b) particles as a function of initial particle size and bed temperature.

Table 4: Kinetic parameters obtained by linear regression with Eqn. 4.

Fluidizing gas	**A_r (s^{-1})**		**E_a (kJ/mol)**		**ψ**	
	BW	PP	BW	PP	BW	PP
Air	0.64	7.5	18.3	32.0	0.82	0.80
Nitrogen	0.12	3.3	10.6	27.5	0.98	0.87

In general, the devolatilization time is shorter under oxidizing conditions. As observed by Bu et al. [77], the transfer of oxygen from the surrounding to the surface of the particle provides the ignition of the char formed during the last devolatilization stage of the biomass. The heat released by the char

365 combustion enhances the heating rate of the particle, promoting the endothermic decomposition of
366 the solid biomass. This effect can be observed from the higher pre-exponential factor when air is used
367 as fluidizing medium, which shows more than 100% increase for both materials when oxygen is
368 present. However, the presence of oxygen also leads to an increase of the apparent activation energy
369 needed for the devolatilization. The same behaviour has been reported by several TGA
370 (thermogravimetric analysis) studies [78,79], which show that the activation energy increases when
371 operating in oxidizing conditions. This reduction of the overall reactivity can be attributed to the
372 additional resistance to mass transfer caused by oxygen and combustion products at the particle
373 surface, which may hinder the transport of volatiles from the porous matrix of char to the surrounding.
374 Furthermore, the heat released by the combustion of oxygen may increase the temperature on the
375 surface of the char, leading to sintering phenomena and subsequent occlusion of the pores of its
376 external layer [80,81]. This reduction of porosity might further increase the resistance to mass transfer
377 of volatiles to the exterior of the particle and explain the higher activation energy. The same trend of
378 kinetic parameters can be observed for polypropylene. However, for this material the values shown
379 in Table 4 are higher than those obtained from beech wood. The greater activation energy can be
380 attributed to the formation of molten layers which obstruct the evolution of volatiles [82]. This
381 observation can be also supported by X-ray visualizations and is better discussed in the next section.
382 In addition, the greater pre-exponential factors may be due to the linear structure of polypropylene
383 molecules, whose thermal cracking is encouraged and more frequent than the more complex
384 constituents of biomass (i.e., cellulose, hemicellulose and lignin).

385 The results of devolatilization time for beech wood obtained in this work are in line with the
386 findings present in literature, as shown in Table 5. As can be seen, obtaining a comprehensive
387 comparison for polypropylene is not straightforward, due to the lack of data.

388

389 Table 5: Devolatilization time data for beech wood and polypropylene in fluidized bed.

Bed Temperature (°C)	Particle size range (mm)	Fluidizing gas	Devolatilization time range (s)	Material	Ref.
439 - 834	2 - 10	Nitrogen	7.4 - 86	BW	[83]
770	6	Air	21.5	BW	[84]
560 - 740	5 - 20	Nitrogen	33 - 201	BW	[54]
500 - 650	8 - 12	Air Nitrogen	30 – 70 60 – 112	BW	This work
850	4	N.A.	10	PP	[10]
500 - 650	8 - 12	Air Nitrogen	40 – 150 50 – 174	PP	This work

390

391

392 3.2 Assessment of volatile matter release within the bed

393 Several authors observed the release of volatiles from a fuel particle in form of bubbles, which
394 contribute to the axial segregation of the particle itself towards the bed surface [21–23,85]. The
395 following sections report a qualitative and quantitative assessment of the effect of operating
396 conditions and feedstock properties on the release of endogenous bubbles.

397

398 3.2.1 Effect of temperature and feedstock properties

399 The lift force induced by the endogenous bubbles on the fuel particle has been quantitatively
400 assessed by Solimene et al.[30], who assumed that the volume of the endogenous bubble at the
401 detachment time is equal to that of the particle. However, experimental observations from this work
402 show that the volume of the endogenous bubbles at the edge of detachment depends on both bed
403 temperature and reacting material. Figure 7 shows the endogenous bubbles diameter at the

404 detachment time measured from X-ray images at the operating conditions studied. In all the
405 experimental runs the polypropylene particle did not rise up to the surface. Thus, for a consistent
406 comparison between the two materials, the measures of the bubble diameter have been carried out
407 according to the greatest residence time obtained from the beech wood experiments (2.3 seconds).

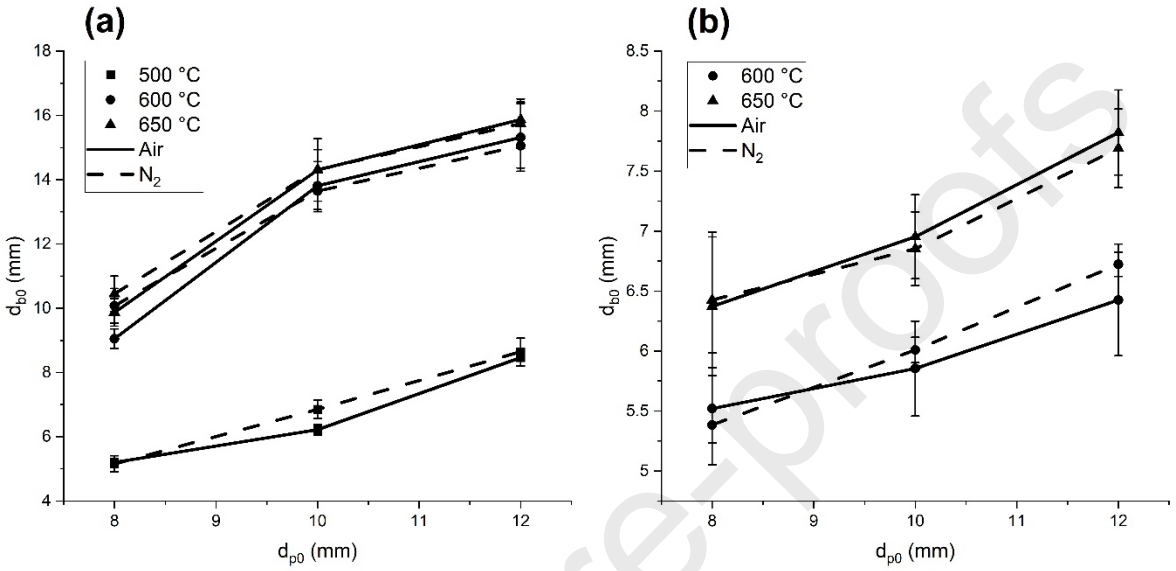

408

409 Figure 7: Measured diameter of endogenous bubble at the detachment time as a function of the initial
410 particle size and temperature for beech wood (a) and polypropylene (b).

411 The endogenous bubble diameter increases with both initial particle size and temperature. For the
412 beech wood particle (Figure 7-a), the bubble diameter is always smaller than the particle diameter at
413 500 °C, while it becomes bigger at the highest temperatures considered. This can be due to the
414 increasing devolatilization rate at high temperatures, which results in a more vigorous release of
415 bubbles. In these conditions the evolution of volatiles can be fast enough to allow coalescence of
416 different endogenous bubbles just above the particle. This phenomenon can be considered similar to
417 the vertical coalescence of different bubbles from an orifice, where the extent of coalescence increases
418 with the gas flowrate [58]. Moreover, the occurrence of bubble coalescence is naturally random
419 [86,87], which explains the higher variability obtained from the measures at 600 and 650 °C.

420 Interestingly, the plastic particle shows a very different behaviour (Figure 7-b). The evolution of
421 volatiles is not visible at 500 °C. The same observation is reported by Fiorentino et al. [22] about the

pyrolysis of TDF (tyre derived fuel) at temperature below 700 °C. According to the authors, this can be due to the slow devolatilization rate, which is unable to generate bubbles and all the volatiles released percolate through the emulsion phase. The formation of endogenous bubbles can be observed at 600 and 650 °C and their size at the detachment time is always smaller than that of the particle. The reason of such behaviour may be due to an additional melting step of polymeric materials. Different authors have already observed the formation of wet aggregates of molten plastic and sand in fluidized beds [73,88]. This layer of unfluidized sand may generate a resistance to transport phenomena and hinder the rapid evolution of volatiles. Similarly, Biagini et al. [82] observed that melting and devolatilization can occur simultaneously at high heating rates and the volatiles are released from the inner of the particle into its outer molten and viscous regions. This results in a further limitation of mass transfer rate. In general, the endogenous bubbles released from polypropylene are always smaller than those obtained from devolatilization of beech wood. This result is in line with the assumption of naphthalene and phenol as lumped components representing the volatiles released from PP and BW, respectively. Assuming that the mass flow rate of devolatilization is similar for both materials, the higher molecular weight of naphthalene leads to a lower volumetric flow rate, hence a smaller endogenous bubble size. Due to the scarcity of information in the present literature, however, the behaviour of polymeric materials in fluidized beds during thermal decomposition requires a deeper investigation.

3.2.2 Effect of fluidizing medium

Figure 7 also shows a surprising result. The size of the endogenous bubbles at the detachment time is independent of the fluidizing medium used for both materials. Under oxidizing condition, the fast homogeneous chemical reaction between the bulk oxygen and volatiles should increase the number of moles of gas released, and therefore the volume of endogenous bubbles. This would result in a greater momentum transferred to the particle [30]. However, according to the experimental observations, the oxidation of volatiles either occurs at a later stage, after the volatile species have

448 been released from the fuel particle and formed endogenous bubbles or is not significant within the
449 dense bed. A possible explanation of this behaviour is proposed in the following discussion. As
450 already mentioned, the release of an endogenous bubble from a decomposing solid particle can be
451 assumed as the same of a volatile matter bubble just above an orifice in a bed at minimum fluidization.
452 According to the gas interchange theory [58], the oxidation of the volatile molecules takes place after
453 the transfer of oxygen from the bed emulsion to the bubble cloud and, ultimately, from the cloud to
454 the bubble. Figure 8 shows a schematic of the interchange phenomenon.
455

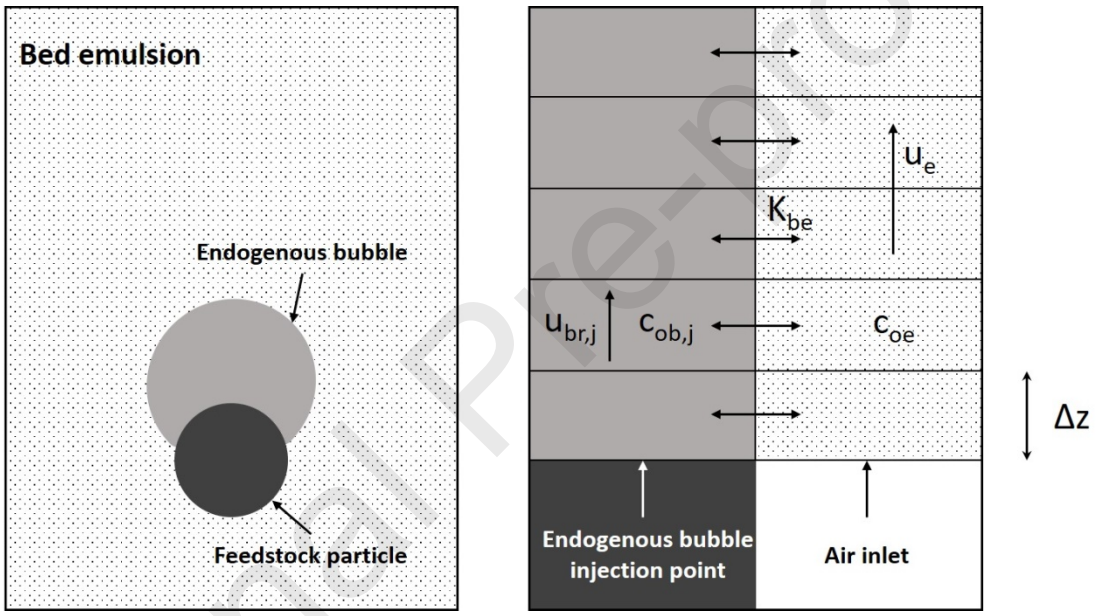

456
457 Figure 8: Oxygen transfer between emulsion and endogenous bubbles along the bed height.
458
459 The concentration gradient of oxygen from the emulsion to the bubble phase along the axial
460 position z is given by:

$$u_{br}\frac{dc_{ob}}{dz} = K_{be}(c_{oe} - c_{ob}) \qquad (33)$$

461
462 where u_{br} is the bubble velocity, while c_{ob} and c_{oe} are the concentration of oxygen in the bubble and
463 emulsion, respectively. All the equations used for the discussion are reported in Supplementary

material. The integration of Eqn. 33 for the j^{th} bubble from its initial position $z = z_j$ to the detachment position $z = z_{0,j}$, leads to:

$$c_{ob,j} = c_{oe}\left(1 - e^{-K_{be,j}\frac{(z_{0,j} - z_j)}{u_{br,j}}}\right) = c_{oe}\left(1 - e^{-K_{be,j}\,\Delta t_{0,j}}\right) \quad (34)$$

For the integration it was assumed that the concentration of oxygen in the bubble as soon as it forms is zero. The ratio between displacement and velocity is equal to the elapsed time needed by the bubble to detach from the particle, defined as:

$$\Delta t_{0,j} = t_{0,j} - t_{0,j-1} \quad (35)$$

where $t_{0,j-1}$ is the detachment time of the bubble j-1, which is assumed to be equal to the formation time of the bubble j.

It is possible to compare the time scale of the phase interchange with that of volatiles oxidation by the investigation of the following Damköhler number for each bubble released:

$$Da_{0,j} = \frac{Reaction\,rate\,O_2 - volatile}{Convective\,mass\,transfer\,rate\,emulsion - bubble} = \frac{V_{b0,j}\,k_{vm}\,c_{ob,j}\,c_{vm,j}}{S_{be,j}\,k_{be,j}\,(\,c_{oe} - \,c_{ob,}} \quad (36)$$

Eqn. 36 can be manipulated to obtain:

$$Da_{0,j} = \frac{k_{vm}\,c_{vm,j}\left(e^{K_{be,j}\,\Delta t_{0,j}} - 1\right)}{K_{be,j}} \quad (37)$$

The assessment of the Damköhler number allows to distinguish between two extreme regimes:

1. Da << 1: The time needed for the oxidation of the volatiles bubble is much higher than the transfer time of O_2 from the emulsion to the bubble. The chemical reaction is the controlling mechanism.

2. Da >> 1: The time needed for the oxidation of the volatiles bubble is much lower than the transfer time of O_2 from the emulsion to the bubble. The convective mass transfer is the controlling mechanism.

Eqn. 37 was solved iteratively for each endogenous bubble released at the detachment position from the induction time to the end of devolatilization for all the conditions studied. Figure 9 shows the results obtained from the computation for both beech wood and polypropylene particles. The Damköhler number reported in the graph is averaged for all the bubbles produced along the highest residence time obtained from the biomass experiments (2.3 seconds) for a consistent comparison.

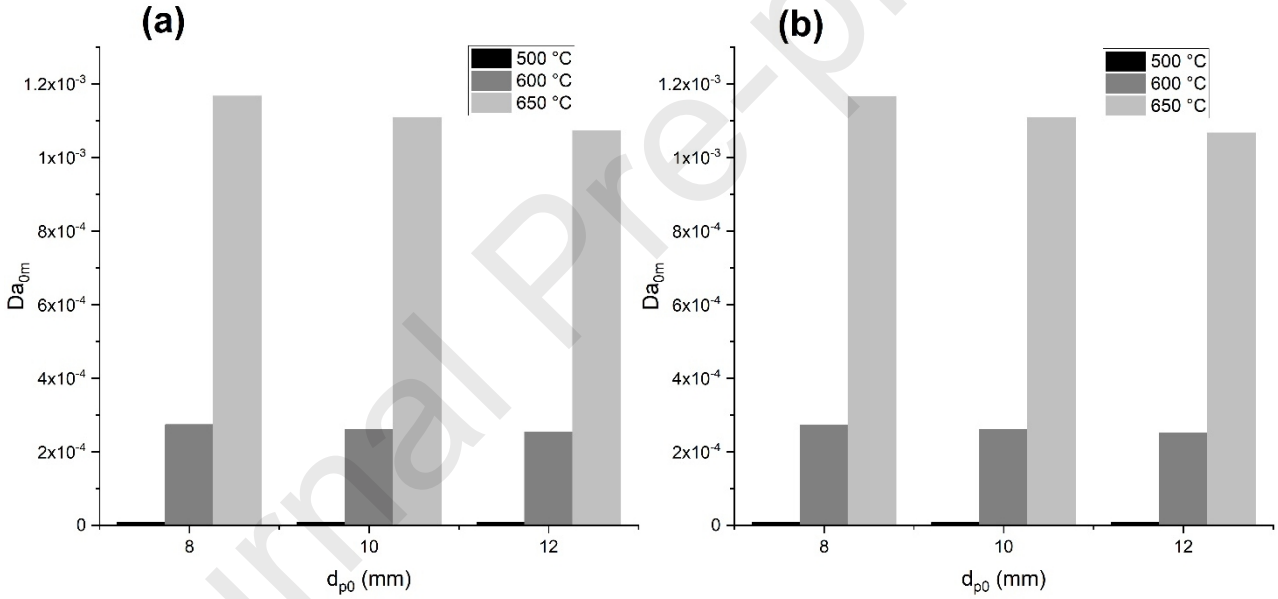

Figure 9: Averaged Damköhler number of endogenous bubbles at the detachment time as a function of initial particle size for beech wood (a) and polypropylene (b).

Very small values of Da_{0m} suggest that the phenomenon is controlled by the oxidation reaction ($Da_{0m} << 1$). This demonstrates the behaviour observed in Figure 7, where each endogenous bubble released from the particle is unable to react with the oxygen from the emulsion phase. Furthermore, the present observations can be extended along the whole height of the bed, considering the growth of the bubble as a function of the axial position. Figure 10 shows the values of the Damköhler number

497 Da_z for the last released bubble from the smallest particle at the highest temperature studied. This
498 choice is justified from the trend in Figure 9, where Da_{0m} increases with temperature and with
499 decreasing particle size. This means that if the condition $Da_z << 1$ is true in this limiting case, then it
500 is also true in all the other conditions considered in this study.
501

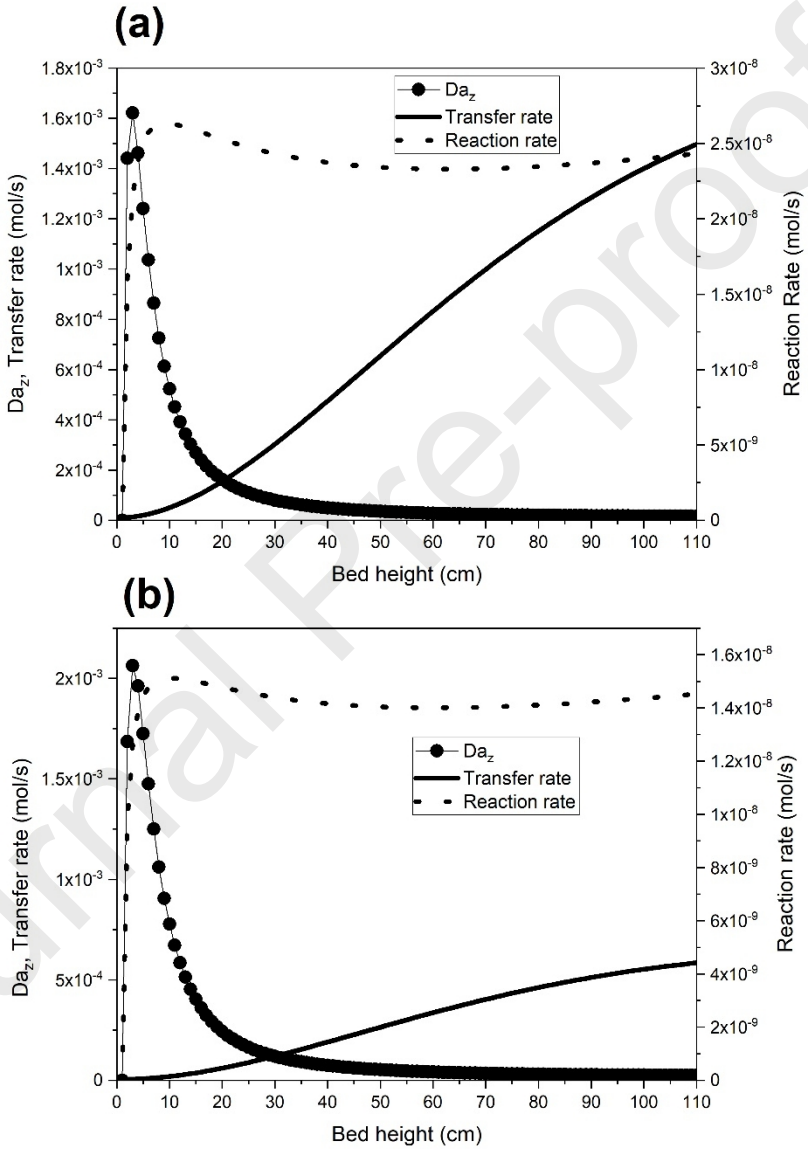

502
503 Figure 10: Damköhler number along the bed height in a pilot scale fluidized bed and for a particle of 8
504 mm at 650 °C, for beech wood (a) and polypropylene (b).
505
506 The fluidized bed used in the experiments is relatively shallow, but the simulation in Figure 10 has
507 been carried out for a bed height of 110 cm and bed diameter of 25 cm, to closely mirror industrial

applications [61]. It can be noted from the graph that the chemical reaction controlling regime is still verified, as the transfer rate is always greater than the reaction rate along the whole bed height. Da_z increases up to a maximum value at 3 cm from the bottom for both BW and PP. This is due to the faster increase of the reaction rate near the bottom of the bed because of the small endogenous bubble volume. After this point, the reaction rate starts decreasing to a nearly constant value, while the continuous increase of the interchange transfer rate takes place due to the expansion of the bubbles along the height of the bed. This finding is very important as it confirms that the volatile matter bypasses the fluidized solids regardless of the oxidizing nature of the surrounding and reacts into the freeboard of the reactor, as reported by Salatino and Solimene [10]. In addition, when more particles are present, the coalescence between more frequent endogenous bubbles and fluidizing agent might become important and further increase the extent of volatile bypass. However, these results must be considered with caution in the case of improved mixing (e.g., vigorous bubbling/slugging regime, circulating fluidized beds) and higher temperatures, when faster oxidation takes place. The investigation of the Damköhler number might be helpful to find an optimal combination of operating conditions, in order to design more efficient operations for thermochemical conversions of biomass and waste in fluidized bed reactors.

3.2.3 Determination of the endogenous bubbles lift effect

In the following section a correlation is proposed for a more accurate estimate of the endogenous bubble size at the detachment time. Equations 11 and 12 significantly underestimates the measured bubbles diameter, as they do not take into account the vertical coalescence that can occur between two or more bubbles as the gas flowrate through the orifice increases [58]. Nguyen and Leung [89] noted that the actual volume of the bubbles can be estimated by considering a proportionality constant obtained from experimental data. Thus, Eqn. 12 for a single bubble can be rewritten as follows:

$$V_{b0} = \gamma\, Q\, t_0 - \qquad (38)$$

532 From a force balance on the bubble, the criterion for the detachment is [90]:

$$\frac{1}{2} g\, t_0^2 = \frac{d_{b0}}{2} \qquad (39)$$

533

534 which means that the bubble detaches when the displacement is equal to its radius. The solution of
535 the two equations leads to:

$$d_{b0} = 1.259\, \gamma^{0.4} \frac{Q^{0.4}}{g^{0.2}} \qquad (40)$$

536

537 The above equation makes sense as long as the particle is immersed within the bed, because the
538 volatiles are not released anymore in form of bubbles when it reaches the surface. Thus, Eqn. 40
539 becomes:

$$d_{b0} = 1.259\, \gamma^{0.4} \frac{\left(\frac{m_{p0}\, w}{\rho_{vm}} k e^{-kt_s}\right)^{0.4}}{g^{0.2}} \qquad (41)$$

540

541 For highly volatile feedstock in fluidized bed reactors, the residence time (or axial segregation
542 time) t_s of the particles is relatively low compared to the whole devolatilization stage. As a
543 consequence, the term e^{-kts} approaches to 1 and the bubble diameter only depends on the temperature
544 and feedstock properties. It is important to note that this assumption cannot be applied to
545 polypropylene in the range of operating conditions studied, since the particles remained within the
546 bed for the whole decomposition period. This behaviour will be better discussed in the next section.
547 In addition, this approximation might lead to inconsistencies in vigorous bubbling and circulating
548 fluidized beds, when the mixing between bed material and solid fuel is promoted.

549 Manipulation of Eqn. 41 gives:

$$d_{b0}\, \tau^{0.4} = 1.259\, \frac{\gamma^{0.4}}{g^{0.2}} \left(\frac{\pi\, \rho_{p0}\, w\, R\, T}{6\, P\, M_{vm}}\right)^{0.4} d_{p0}^{1.2} \qquad (42)$$

550

where $\tau = 1/k$ is the devolatilization time constant. From a linear regression on the experimental data of d_{b0} and τ, it is possible to obtain the values of γ at each temperature considered. Figure 11 shows experimental data along with the fitting curves from Eqn. 42.

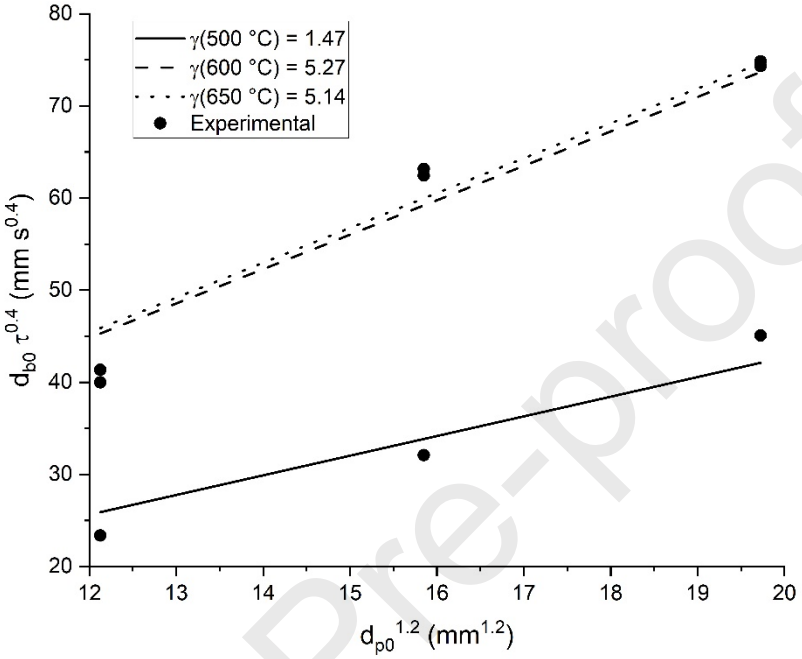

Figure 11: Experimental and calculated LHS of Eqn. 42 as a function of $d_{p0}^{1.2}$.

The predictions are in good agreement with the experimental observations ($R^2 = 0.88$). A more accurate estimate of the endogenous bubble size can be useful from a practical point of view, in order to improve mixing and segregation models in fluidized beds during thermochemical conversions. Solimene et al. [30] proposed the following correlation for the computation of the lift force:

$$F_{lift} = 0.586\,\omega\,\rho_e\,g^{0.6}\,d_p\,Q^{0.8} = 0.372\,\rho_e\,g^{0.6}\,d_p\,Q^{0.8} \qquad (43)$$

Following the same procedure described by the authors, and using Eqn. 42 and the correlation for the rise velocity of a single bubble [58], it is possible to write:

$$F' = 0.798\ \omega\ \rho_e\ g^{0.4}\ \gamma^{1.2}\ Q^{1.2} \qquad (44)$$

566 Dividing Eqn. 44 by Eqn. 43, the modified lift force is:

$$F' = 1.36\ \frac{\gamma^{1.2}\ Q^{0.4}}{d_p\ g^{0.2}}\ F_{lift} \qquad (45)$$

567 In the following sections, the model described in section 2 and corrected with equations 42 and 45
568 is referred as revised model.
569

570 3.3 Validation of segregation model

571 The computation results reported below were obtained using the kinetic parameters from
572 experiments in inert condition, since the release of volatiles within the bed is not affected by the
573 properties of the fluidizing medium as previously discussed.
574

575 3.3.1 Biomass particle

576 Figure 12 compares experimental and calculated particle segregation profiles and instantaneous
577 velocity for beech wood particle. The values 0 and 1 on the y-axis in Figure 12-a correspond to the
578 dimensionless feeding point and surface of the bed, respectively.
579

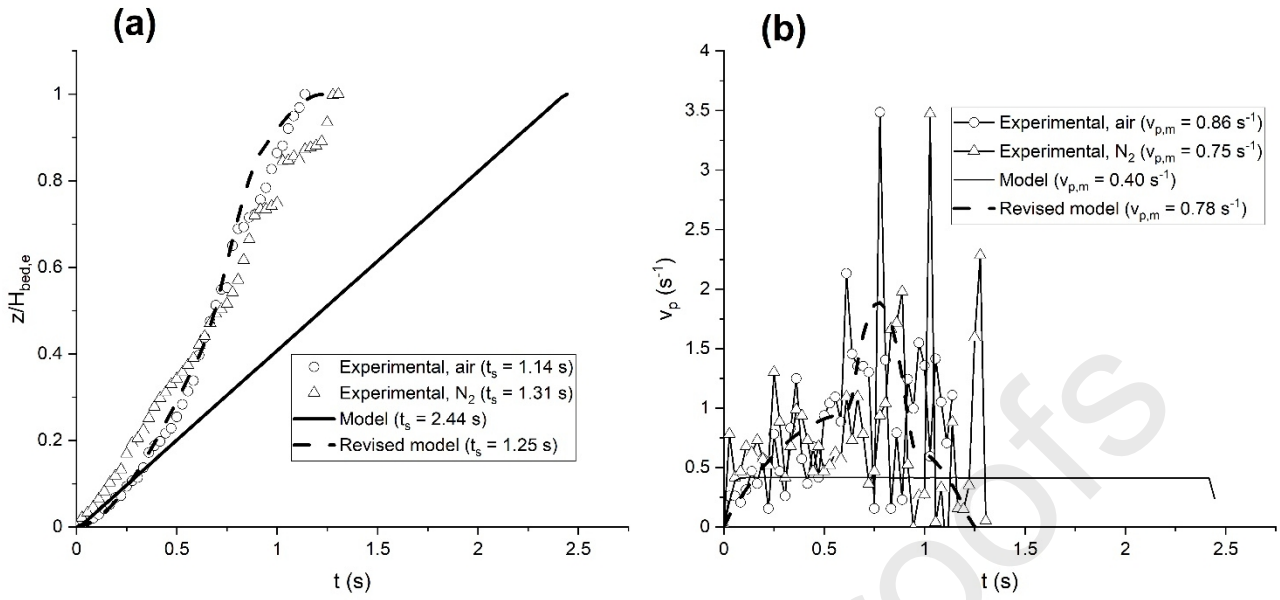

Figure 12: Experimental and calculated axial segregation profile (a) and instantaneous velocity (b) at 600 °C and for a 10 mm diameter beech wood particle.

The significant difference in predictions between the 2 models depends on the expression of the lift force and the detachment criterion for the endogenous bubbles (Figure 12-a). The revised model offers a better estimate of the particle axial trajectory within the bed as it takes into account the bigger size of the bubbles estimated with Eqn. 42, which gives a greater lift effect compared with the first model. The experimental velocity profile shows multiple fluctuations around a mean value (Figure 12-b). This behaviour was observed for the first time by Fiorentino et al. [22,23] and represents the effect of different endogenous bubbles generated by the particle, which increases its velocity in a stepwise fashion during the whole rising time. The velocity increases as the bubble detaches due to the lift effect and decreases while a new bubble is forming. The authors identified this pattern as MBS (Multiple Bubble Segregation), which depends on several factors, including physical properties of both fluidized bed and feedstock.

Further confirmation of the establishment of pattern MBS can be observed in Figure 13, which shows the endogenous bubbles frequency for all the conditions investigated. The value of f_b has been

calculated as the ratio between the number of released volatile bubbles and the residence time of the feedstock particle within the bed.

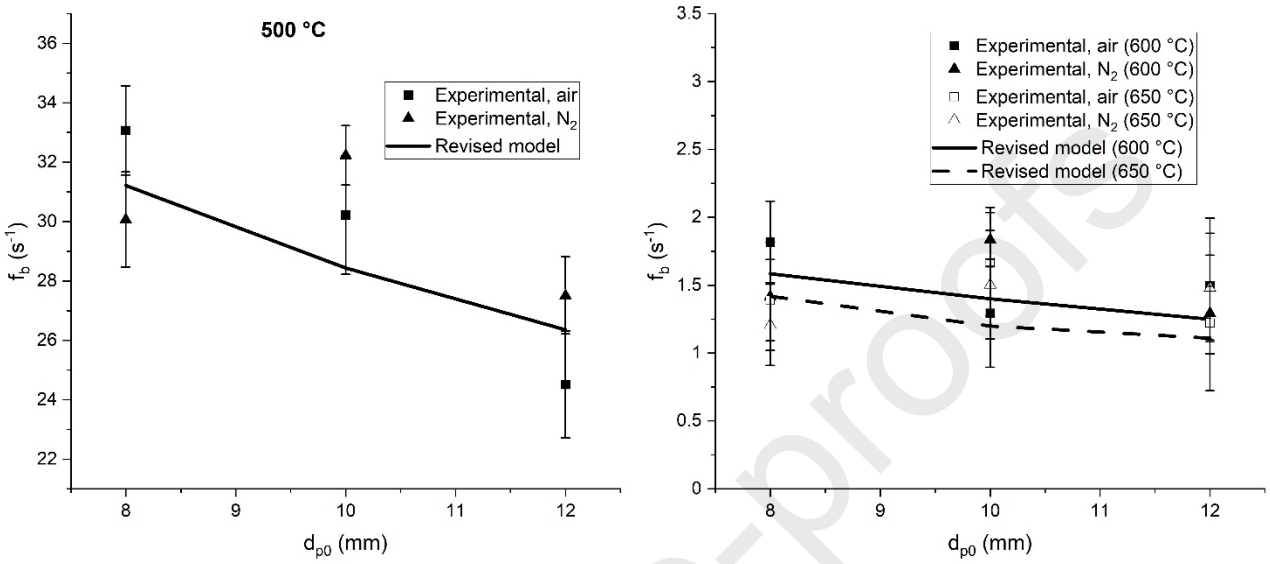

Figure 13: Experimental and calculated endogenous bubbles frequency as a function of initial size of beech wood particle.

The bubble frequency is always higher than unity, confirming the evolution of multiple bubbles during the in-bed particle devolatilization. In general, the values calculated with the model follow a decreasing trend with both initial particle diameter and bed temperature. As previously discussed, endogenous bubbles size increases as these physical parameters increase. As a consequence, according to the detachment criterion described for the computation, a big bubble takes longer to detach from the particle than in case of a small bubble. This results in more endogenous bubbles produced for small particles at low temperatures, and therefore a greater frequency. However, at a given temperature, the fluidizing medium does not affect the bubble frequency for each particle size investigated. This result further confirms the lack of correlation between endogenous bubbles size and nature of fluidizing media used in this work.

3.3.2 Plastic particle

Figure 14 shows the segregation profiles for a polypropylene particle. It is worth noting that the revised model was not used in this case. As discussed previously, the proposed correlation for the endogenous bubble size (Eqn. 42) makes sense as long as the particle releases its volatile content mostly into the freeboard (as in the case of biomass particles).

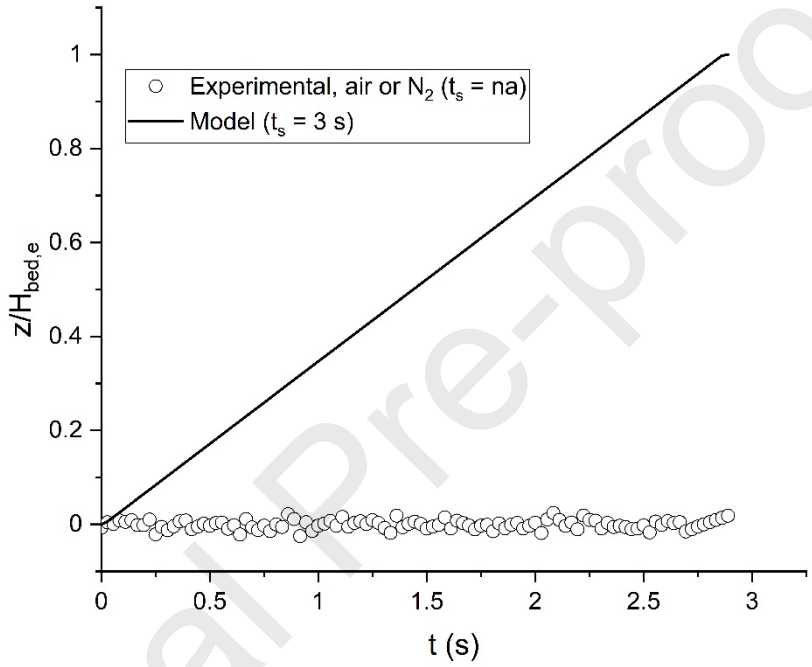

Figure 14: Experimental and calculated axial segregation profile at 600 °C and for a 10 mm diameter polypropylene particle.

In this case the particle was never observed to rise, for all conditions investigated, and the model fails in the prediction of the particle motion. Similar behaviour is reported by Fiorentino et al. [23] for TDF at temperatures below 700 °C. According to the authors, the kinetics of devolatilization is not fast enough to generate endogenous bubbles capable to lift the particle up to the surface of the bed. However, this is an unexpected behaviour. Since all the particles investigated in this study are buoyant, they should rise regardless of the effect of devolatilization, as predicted by the model. Similar observations are shown by Baron et al. [88], who reported that polymer pellets sink quickly after over-bed feeding. The authors concluded that the unfluidized sand present on the upper surface

of the polymer particle increases its density, which can exceed that of the emulsion phase. Nevertheless, more effort is needed to better understand thermal and dynamic behaviour of plastic materials in fluidized bed reactors. This may support the development of more effective technologies for the exploitation of plastic waste.

4. Conclusions

This work investigated the devolatilization behaviour of a single feedstock particle in a lab-scale fluidized bed reactor at high temperatures by means of a non-invasive X-ray imaging technique. The highly volatile materials used in the study were chosen in order to resemble the main constituents of RDF feedstock, namely biomass and plastic. A single particle of either beech wood or polypropylene was fed into the reactor and both dynamic behaviour and kinetics of devolatilization were characterized. Results did show that these two features are closely connected. The use of gas analyser measurements provided a comprehensive assessment of the devolatilization behaviour, which was found to be highly affected by the fluidizing medium for both materials investigated. Pre-exponential factor and activation energy appeared to be very sensitive to the presence of oxygen, and were generally higher when air was used as fluidizing gas. The overall devolatilization time was found to be in the range of 30-112 seconds and 40-174 seconds for beech wood and polypropylene, respectively. Interestingly, the in-bed release of volatiles appeared to be independent of the presence of oxygen in the fluidizing medium. This finding was supported by visual evidence provided by X-ray images, which showed that endogenous bubbles size and frequency are independent of fluidizing gas properties. This behaviour was attributed to the controlling oxidation mechanisms of the volatile matter released, as demonstrated by the investigation of the Damköhler number from the interchange phase theory of oxygen between emulsion phase and endogenous bubbles.

A one-dimensional model was developed to predict the dynamic behaviour of the reacting particle within the bed. The model takes into account both motion and thermal degradation of the particle in order to provide a comprehensive description of the phenomenon. The assumption of endogenous

bubble formation and detachment from a single orifice was proven extremely effective to compute the lift effect acting on the particle, due to its ease of implementation. Because of the knowledge about endogenous bubbles size provided by the X-ray imaging technique, a revised version of the model was proposed. Model results were in good agreement with experimental observations for the biomass feedstock, which follows the MBS segregation pattern at the conditions investigated. The main limitation of the model was its failure to predict the behaviour of the plastic particles. The peculiar behaviour observed for this material was associated with its completely different mechanism of degradation, where the melting step was believed to have a great impact on both volatiles release and particle motion within the bed. The change in particle physical properties and formation of dense plastic-sand agglomerates might be responsible for the behaviour of this material. However, further investigation is needed to better understand the mechanism of plastic decomposition in fluidized beds.

This work confirmed the importance of developing systematic methodologies for the investigation of single particle devolatilization which, at present, appears to be the most effective approach to gain deeper insight on the interaction between feedstock and fluidized bed during thermochemical conversions. This is a central aspect for future development and exploitation of novel technologies, as well as improvement of existing ones, for thermal treatments of waste feedstock.

Acknowledgment

The authors wish to acknowledge Dr Domenico Macrì for his help with providing the scripts for the image analysis and Zach Bond for sharing thoughts and knowledge about gas analysis measurements.

Nomenclature

Symbols	
A	Pre-exponential factor

c [mol/m^3]	Molar concentration
Da	Damköhler number
d [m]	Diameter
E_a [J/mol]	Activation energy
F´ [N]	Revised lift force
f [s^{-1}]	Frequency
g [m/s^2]	Gravitational acceleration
$H_{bed,e}$ [m]	Height of expanded bed
h [W/m^3 K]	Heat transfer coefficient
K_{be} [s^{-1}]	Interchange coefficient bubble-emulsion
k [s^{-1}]	Reaction rate constant
k_g [m/s]	Mass transfer coefficient in gas phase
k_{be} [m/s]	Mass transfer coefficient bubble-emulsion
M [kg/mol]	Molecular weight
m [kg]	Mass
P [Pa]	Pressure
Q [m^3/s]	Volumetric flow rate of volatiles
r [m]	Radius
R [J/mol K]	Universal gas constant
S_{be} [m^2]	Exchange surface bubble-emulsion
T [K]	temperature
w	Mass composition of volatile matter in feedstock
X	Mass conversion of solid feedstock
u [m/s]	Velocity
u_{br} [m/s]	Rise velocity of a single bubble
V [m^3]	Volume
y	Molar fraction
z [m]	Axial position
Greek letters	
α [m^2/s]	Thermal diffusivity of solid feedstock
β	Stoichiometric coefficient of char combustion
γ	Proportional constant in Eqn. 38
ε	Void fraction
ϵ	Emissivity
λ [W/m K]	Thermal conductivity of solid feedstock
ρ [kg/m^3]	Density
σ [W/m^2 K^4]	Stefan-Boltzmann constant
τ [s]	Devolatilization time constant
ψ	Exponent in Eqn. 3
ω	Proportional constant in Eqn. 43
Subscripts	
0	Initial or detachment time of endogenous bubble

b	Endogenous bubble
c	Char of feedstock particle
d	Devolatilization
e	Emulsion phase
eff	Effective
f	Fluidizing gas
g	Gas phase
i	Number of feedstock particle sizes
in	Induction
j	Endogenous bubble number
m	Averaged
mf	Minimum fluidization
o	Oxygen
p	Particle
r	Reference value of particle size
s	Segregation or residence
t	Lead tracer
v	Virgin core of feedstock particle
vm	Volatile matter

Acronyms	
BW	Beech wood
EC	Electrochemical
IR	Infrared
LHS	Left hand side
MBS	Multiple Bubble Segregation
MSW	Municipal solid waste
PP	Polypropylene
RDF	Refuse derived fuel
ROI	Region of interest

References

[1] M. Shumal, A.R. Taghipour Jahromi, A. Ferdowsi, S.M. Mehdi Noorbakhsh Dehkordi, A. Moloudian, A. Dehnavi, Comprehensive analysis of municipal solid waste rejected fractions as a source of Refused Derived Fuel in developing countries (case study of Isfahan- Iran): Environmental Impact and sustainable development, Renew. Energy. 146 (2020) 404–413. https://doi.org/10.1016/j.renene.2019.06.173.

[2] P. Rajca, A. Poskart, M. Chrubasik, M. Sajdak, M. Zajemska, A. Skibiński, A. Korombel, Technological and economic aspect of Refuse Derived Fuel pyrolysis, Renew. Energy. 161 (2020) 482–494. https://doi.org/10.1016/j.renene.2020.07.104.

[3] B. Leckner, F. Lind, Combustion of municipal solid waste in fluidized bed or on grate – A comparison, Waste Manag. 109 (2020) 94–108. https://doi.org/10.1016/j.wasman.2020.04.050.

[4] J. Fuchs, J.C. Schmid, S. Müller, H. Hofbauer, Dual fluidized bed gasification of biomass with selective carbon dioxide removal and limestone as bed material: A review, Renew. Sustain. Energy Rev. 107 (2019) 212–231. https://doi.org/10.1016/j.rser.2019.03.013.

[5] M.M. Jaffar, M.A. Nahil, P.T. Williams, Synthetic natural gas production from the three stage (i) pyrolysis (ii) catalytic steam reforming (iii) catalytic hydrogenation of waste biomass, Fuel Process. Technol. 208 (2020) 106515. https://doi.org/10.1016/j.fuproc.2020.106515.

[6] G. Amaya-Santos, S. Chari, A. Sebastiani, F. Grimaldi, P. Lettieri, M. Materazzi, Biohydrogen: A life cycle assessment and comparison with alternative low-carbon production routes in UK, J. Clean. Prod. 319 (2021) 128886. https://doi.org/10.1016/j.jclepro.2021.128886.

[7] M. Materazzi, P.U. Foscolo, The role of waste and renewable gas to decarbonize the energy sector, in: Substit. Nat. Gas from Waste, Elsevier, 2019: pp. 1–19. https://doi.org/10.1016/B978-0-12-815554-7.00001-5.

[8] Q. He, Q. Guo, K. Umeki, L. Ding, F. Wang, G. Yu, Soot formation during biomass gasification: A critical review, Renew. Sustain. Energy Rev. 139 (2021) 110710. https://doi.org/10.1016/j.rser.2021.110710.

[9] H. Hofbauer, M. Materazzi, Waste gasification processes for SNG production, in: Substit. Nat. Gas from Waste, Elsevier, 2019: pp. 105–160. https://doi.org/10.1016/B978-0-12-815554-7.00007-6.

[10] P. Salatino, R. Solimene, Mixing and segregation in fluidized bed thermochemical conversion of biomass, Powder Technol. 316 (2017) 29–40. https://doi.org/10.1016/j.powtec.2016.11.058.

[11] G. Martinez Castilla, A. Larsson, L. Lundberg, F. Johnsson, D. Pallarès, A novel experimental method for determining lateral mixing of solids in fluidized beds – Quantification of the splash-zone contribution, Powder Technol. 370 (2020) 96–103. https://doi.org/10.1016/j.powtec.2020.05.036.

[12] D. Müller, T. Plankenbühler, J. Karl, A Methodology for Measuring the Heat Release Efficiency in Bubbling Fluidised Bed Combustors, Energies. 13 (2020) 2420. https://doi.org/10.3390/en13102420.

[13] M. Suárez-Almeida, A. Gómez-Barea, C. Pfeifer, B. Leckner, Fluid dynamic analysis of dual fluidized bed gasifier for solar applications, Powder Technol. 390 (2021) 482–495. https://doi.org/10.1016/j.powtec.2021.05.032.

[14] A. Ramos, E. Monteiro, V. Silva, A. Rouboa, Co-gasification and recent developments on waste-to-energy conversion: A review, Renew. Sustain. Energy Rev. 81 (2018) 380–398. https://doi.org/10.1016/j.rser.2017.07.025.

[15] I. Mema, K.A. Buist, J.T. Padding, Fluidization of spherical versus elongated particles : Experimental investigation using magnetic particle tracking, (2020) 1–13. https://doi.org/10.1002/aic.16895.

[16] I. Mema, J.T. Padding, Spherical versus elongated particles – Numerical investigation of mixing characteristics in a gas fluidized bed, Chem. Eng. Sci. X. 8 (2020) 100079. https://doi.org/10.1016/j.cesx.2020.100079.

[17] Y. Bai, H. Si, Experimental study on fluidization, mixing and separation characteristics of binary mixtures of particles in a cold fluidized bed for biomass fast pyrolysis, Chem. Eng. Process. - Process Intensif. 153 (2020) 107936. https://doi.org/10.1016/j.cep.2020.107936.

[18] L.-J. Wang, G.-C. Wei, S.-P. Duan, Q.-F. Hou, CFD-DEM study on the mixing characteristics of binary particle systems in a fluidized bed of refuse-derived fuel, Part. Sci. Technol. 37 (2019)

736 51–59. https://doi.org/10.1080/02726351.2017.1338320.

737 [19] B. Szücs, P. Szentannai, Experimental Investigation on Mixing and Segregation Behavior of
738 Oxygen Carrier and Biomass Particle in Fluidized Bed, Period. Polytech. Mech. Eng. 63 (2019)
739 188–194. https://doi.org/10.3311/PPme.13764.

740 [20] M. Urciuolo, R. Solimene, P. Ammendola, S. Krusch, V. Scherer, P. Salatino, R. Chirone, O.
741 Senneca, On the agglomeration tendency of carbonaceous fuels in fluidized beds, Fuel. 277
742 (2020) 118187. https://doi.org/10.1016/j.fuel.2020.118187.

743 [21] G. Bruni, R. Solimene, A. Marzocchella, P. Salatino, J.G. Yates, P. Lettieri, M. Fiorentino, Self-
744 segregation of high-volatile fuel particles during devolatilization in a fluidized bed reactor,
745 Powder Technol. 128 (2002) 11–21. https://doi.org/10.1016/S0032-5910(02)00149-3.

746 [22] M. Fiorentino, A. Marzocchella, P. Salatino, Segregation of fuel particles and volatile matter
747 during devolatilization in a fluidized bed reactor - II. Experimental, Chem. Eng. Sci. 52 (1997)
748 1909–1922. https://doi.org/10.1016/S0009-2509(97)00019-5.

749 [23] M. Fiorentino, A. Marzocchella, P. Salatino, Segregation of fuel particles and volatile matter
750 during devolatilization in a fluidized bed reactor - I. Model development, Chem. Eng. Sci. 52
751 (1997) 1893–1908. https://doi.org/10.1016/S0009-2509(97)00018-3.

752 [24] F. Scala, Fluidized Bed Technologies for Near-Zero Emission Combustion and Gasification,
753 2013. https://doi.org/10.1533/9780857098801.

754 [25] K.S. Jaya Bharathi. J., Hydrodynamics and Particle Mixing Characteristics of a Ternary Mixture
755 in a Gas-Solid Fluidized Bed, Int. J. Recent Technol. Eng. 8 (2019) 2520–2526.
756 https://doi.org/10.35940/ijrte.D7120.118419.

757 [26] M.S. Alagha, B. Szucs, P. Szentannai, Numerical study of mixing and heat transfer of SRF
758 particles in a bubbling fluidized bed, J. Therm. Anal. Calorim. 142 (2020) 1087–1096.
759 https://doi.org/10.1007/s10973-019-09135-2.

[27] J. Wünning, Flameless oxidation to reduce thermal NO-formation, Prog. Energy Combust. Sci. 23 (1997) 81–94. https://doi.org/10.1016/S0360-1285(97)00006-3.

[28] M. Materazzi, R. Taylor, Plasma-Assisted Gasification for Waste-to-Fuels Applications, Ind. Eng. Chem. Res. 58 (2019) 15902–15913. https://doi.org/10.1021/acs.iecr.9b01239.

[29] A.C. Rees, J.F. Davidson, J.S. Dennis, A.N. Hayhurst, The rise of buoyant fuel-particles in a slugging gas-fluidized combustor, Chem. Eng. Res. Des. 84 (2006) 319–327. https://doi.org/10.1205/cherd05043.

[30] R. Solimene, A. Marzocchella, P. Salatino, Hydrodynamic interaction between a coarse gas-emitting particle and a gas fluidized bed of finer solids, Powder Technol. 133 (2003) 79–90. https://doi.org/10.1016/S0032-5910(03)00080-9.

[31] Z. Yang, L. Duan, L. Li, D. Liu, C. Zhao, Movement and mixing behavior of a single biomass particle during combustion in a hot fluidized bed combustor, Powder Technol. 370 (2020) 88–95. https://doi.org/10.1016/j.powtec.2020.05.037.

[32] A. Köhler, D. Pallarès, F. Johnsson, Modeling Axial Mixing of Fuel Particles in the Dense Region of a Fluidized Bed, Energy and Fuels. (2020). https://doi.org/10.1021/acs.energyfuels.9b04194.

[33] A. Soria-Verdugo, L.M. Garcia-Gutierrez, S. Sanchez-Delgado, U. Ruiz-Rivas, Circulation of an object immersed in a bubbling fluidized bed, Chem. Eng. Sci. 66 (2011) 78–87. https://doi.org/10.1016/j.ces.2010.10.006.

[34] A. Soria-Verdugo, L.M. Garcia-Gutierrez, N. García-Hernando, U. Ruiz-Rivas, Buoyancy effects on objects moving in a bubbling fluidized bed, Chem. Eng. Sci. 66 (2011) 2833–2841. https://doi.org/10.1016/j.ces.2011.03.055.

[35] B. Cluet, G. Mauviel, Y. Rogaume, O. Authier, A. Delebarre, Segregation of wood particles in a bubbling fluidized bed, Fuel Process. Technol. 133 (2015) 80–88.

https://doi.org/10.1016/j.fuproc.2014.12.045.

[36] M. Stein, Y.L. Ding, J.P.K. Seville, D.J. Parker, Solids motion in bubbling gas fluidized beds, Chem. Eng. Sci. 55 (2000) 5291–5300. https://doi.org/10.1016/S0009-2509(00)00177-9.

[37] Y.S. Wong, J.P.K. Seville, Single-Particle Motion and Heat Transfer in Fluidized Beds, 52 (2006) 4099–4109. https://doi.org/10.1002/aic.

[38] F. Fotovat, J. Chaouki, Characterization of the upward motion of an object immersed in a bubbling fluidized bed of fine particles, Chem. Eng. J. 280 (2015) 26–35. https://doi.org/10.1016/j.cej.2015.05.130.

[39] F. Fotovat, R. Ansart, M. Hemati, O. Simonin, J. Chaouki, Sand-assisted fluidization of large cylindrical and spherical biomass particles: Experiments and simulation, Chem. Eng. Sci. 126 (2015) 543–559. https://doi.org/10.1016/j.ces.2014.12.022.

[40] A. Köhler, A. Rasch, D. Pallarès, F. Johnsson, Experimental characterization of axial fuel mixing in fluidized beds by magnetic particle tracking, Powder Technol. 316 (2017) 492–499. https://doi.org/10.1016/j.powtec.2016.12.093.

[41] A. Köhler, D. Pallarès, F. Johnsson, Magnetic tracking of a fuel particle in a fluid-dynamically down-scaled fluidised bed, Fuel Process. Technol. 162 (2017) 147–156. https://doi.org/10.1016/j.fuproc.2017.03.018.

[42] W. Yoshimori, T. Ikegai, K. Uemoto, S. Narita, S. Harada, J. Oshitani, Non - invasive measurement of floating – sinking motion of a large object in a gas – solid fluidized bed, Granul. Matter. 21 (2019) 1–11. https://doi.org/10.1007/s10035-019-0897-3.

[43] H.L. Zhu, Y.S. Zhang, M. Materazzi, G. Aranda, D.J.L. Brett, P.R. Shearing, G. Manos, Co-gasification of beech-wood and polyethylene in a fluidized-bed reactor, Fuel Process. Technol. 190 (2019) 29–37. https://doi.org/10.1016/j.fuproc.2019.03.010.

[44] OECD, Improving Plastics Management : Trends , policy responses , and the role of

international co-operation and trade, Environ. Policy Pap. No. 12. (2018) 20.

[45] E.E. Kwon, S. Kim, J. Lee, Pyrolysis of waste feedstocks in CO2 for effective energy recovery and waste treatment, J. CO2 Util. 31 (2019) 173–180. https://doi.org/10.1016/j.jcou.2019.03.015.

[46] R. Xiao, B. Jin, H. Zhou, Z. Zhong, M. Zhang, Air gasification of polypropylene plastic waste in fluidized bed gasifier, Energy Convers. Manag. 48 (2007) 778–786. https://doi.org/10.1016/j.enconman.2006.09.004.

[47] H. Zhou, A. Meng, Y. Long, Q. Li, Y. Zhang, Classification and comparison of municipal solid waste based on thermochemical characteristics, J. Air Waste Manag. Assoc. 64 (2014) 597–616. https://doi.org/10.1080/10962247.2013.873094.

[48] M. Rabacal, M. Costa, M. Vascellari, C. Hasse, Kinetic modelling of sawdust and beech wood pyrolysis in drop tube reactors using advanced predictive models, Chem. Eng. Trans. 37 (2014) 79–84. https://doi.org/10.3303/CET1437014.

[49] C. Guizani, M. Jeguirim, S. Valin, L. Limousy, S. Salvador, Biomass chars: The effects of pyrolysis conditions on their morphology, structure, chemical properties and reactivity, Energies. 10 (2017). https://doi.org/10.3390/en10060796.

[50] S.C. Bhatia, Biomass gasification, in: Adv. Renew. Energy Syst., Elsevier, 2014: pp. 473–489. https://doi.org/10.1016/B978-1-78242-269-3.50018-8.

[51] E. Esmizadeh, C. Tzoganakis, T.H. Mekonnen, Degradation Behavior of Polypropylene during Reprocessing and Its Biocomposites: Thermal and Oxidative Degradation Kinetics, Polymers (Basel). 12 (2020) 1627. https://doi.org/10.3390/polym12081627.

[52] A. Gomez-Barea, S. Nilsson, F. Vidal Barrero, M. Campoy, Devolatilization of wood and wastes in fluidized bed, Fuel Process. Technol. 91 (2010) 1624–1633. https://doi.org/10.1016/j.fuproc.2010.06.011.

[53] S.A. Scott, J.F. Davidson, J.S. Dennis, A.N. Hayhurst, The devolatilisation of particles of a complex fuel (dried sewage sludge) in a fluidised bed, Chem. Eng. Sci. 62 (2007) 584–598. https://doi.org/10.1016/j.ces.2006.09.023.

[54] N. Jand, P.U. Foscolo, Decomposition of wood particles in fluidized beds, Ind. Eng. Chem. Res. 44 (2005) 5079–5089. https://doi.org/10.1021/ie040170a.

[55] J.C. Wurzenberger, S. Wallner, H. Raupenstrauch, J.G. Khinast, Thermal conversion of biomass: Comprehensive reactor and particle modeling, AIChE J. 48 (2002) 2398–2411. https://doi.org/10.1002/aic.690481029.

[56] K.R. Gaston, M.W. Jarvis, P. Pepiot, K.M. Smith, W.J. Frederick, M.R. Nimlos, Biomass pyrolysis and gasification of varying particle sizes in a fluidized-bed reactor, Energy and Fuels. 25 (2011) 3747–3757. https://doi.org/10.1021/ef200257k.

[57] M. Sreekanth, J. Daniel, V. Karthikeyan, Devolatilization of Wood in Fluidized Beds - A Review of Research on Experiments and Modelling, Int. J. Innov. Sci. Res. 14 (2015) 178–187.

[58] D. Kunii, O. Levenspiel, Fluidization Engineering, second ed., Butterworth-Heinemann, 1991.

[59] S.A. Scott, J.F. Davidson, J.S. Dennis, A.N. Hayhurst, Heat Transfer to a Single Sphere Immersed in Beds of Particles Supplied by Gas at Rates above and below Minimum Fluidization, Ind. Eng. Chem. Res. 43 (2004) 5632–5644. https://doi.org/10.1021/ie0307380.

[60] A. Gómez-Barea, B. Leckner, Modeling of biomass gasification in fluidized bed, Prog. Energy Combust. Sci. 36 (2010) 444–509. https://doi.org/10.1016/j.pecs.2009.12.002.

[61] A. Sebastiani, D. Macrì, K. Gallucci, M. Materazzi, Steam - oxygen gasification of refuse derived fuel in fluidized beds: Modelling and pilot plant testing, Fuel Process. Technol. 216 (2021) 106783. https://doi.org/10.1016/j.fuproc.2021.106783.

[62] E.N. Fuller, P.D. Schettler, J.C. Giddings, A new method for prediction of binary gas-phase diffusion coefficients, Ind. Eng. Chem. 58 (1966) 18–27.

856 https://doi.org/10.1021/ie50677a007.

857 [63] R.H.P. Don W. Green, Perry's Chemical Engineers' handbook, eighth ed., 2007.

858 [64] Ł. Czajkowski, W. Olek, J. Weres, Effects of heat treatment on thermal properties of European
859 beech wood, Eur. J. Wood Wood Prod. 78 (2020) 425–431. https://doi.org/10.1007/s00107-
860 020-01525-w.

861 [65] A. Patti, D. Acierno, Thermal Conductivity of Polypropylene-Based Materials, in: Polypropyl. -
862 Polym. Charact. Mech. Therm. Prop., IntechOpen, 2020.
863 https://doi.org/10.5772/intechopen.84477.

864 [66] C. Bu, D. Pallarès, X. Chen, A. Gómez-Barea, D. Liu, B. Leckner, P. Lu, Oxy-fuel combustion of
865 a single fuel particle in a fluidized bed: Char combustion characteristics, an experimental
866 study, Chem. Eng. J. 287 (2016) 649–656. https://doi.org/10.1016/j.cej.2015.11.078.

867 [67] M. Iqbal, A. Nadeem, M. Butt, Refused derived fuel pellets from municipal solid waste and
868 rice husk, Bangladesh J. Sci. Ind. Res. 54 (2019) 329–338.
869 https://doi.org/10.3329/bjsir.v54i4.44567.

870 [68] C. Sprenger, L.G. Tabil, M. Soleimani, Compression and relaxation properties of municipal
871 solid waste refuse-derived fuel fluff, KONA Powder Part. J. 2018 (2018) 200–208.
872 https://doi.org/10.14356/kona.2018005.

873 [69] H. Rezaei, F.Y. Panah, C.J. Lim, S. Sokhansanj, Pelletization of refuse-derived fuel with varying
874 compositions of plastic, paper, organic and wood, Sustain. 12 (2020) 1–11.
875 https://doi.org/10.3390/su12114645.

876 [70] M. Jewiarz, K. Mudryk, M. Wróbel, J. Fraczek, K. Dziedzic, Parameters affecting RDF-based
877 pellet quality, Energies. 13 (2020) 1–16. https://doi.org/10.3390/en13040910.

878 [71] S. Iannello, S. Morrin, M. Materazzi, Fluidised bed reactors for the thermochemical
879 conversion of biomass and waste†, KONA Powder Part. J. 37 (2020) 114–131.

https://doi.org/10.14356/kona.2020016.

[72] A.N. Hayhurst, M.S. Parmar, Does solid carbon burn in oxygen to give the gaseous intermediate CO or produce CO2 directly? Some experiments in a hot bed of sand fluidized by air, Chem. Eng. Sci. 53 (1998) 427–438. https://doi.org/10.1016/S0009-2509(97)00334-5.

[73] F. Burgess, P.D.W. Lloyd, P.S. Fennell, A.N. Hayhurst, Combustion of polymer pellets in a bubbling fluidised bed, Combust. Flame. 158 (2011) 1638–1645. https://doi.org/10.1016/j.combustflame.2010.12.027.

[74] J.S. Dennis, R.J. Lambert, A.J. Milne, S.A. Scott, A.N. Hayhurst, The kinetics of combustion of chars derived from sewage sludge, Fuel. 84 (2005) 117–126. https://doi.org/10.1016/j.fuel.2004.08.020.

[75] S. Rapagnà, G. Mazziotti di Celso, Devolatilization of wood particles in a hot fluidized bed: Product yields and conversion rates, Biomass and Bioenergy. 32 (2008) 1123–1129. https://doi.org/10.1016/j.biombioe.2008.02.010.

[76] D. Macrì, S. Sutcliffe, P. Lettieri, Fluidized bed sintering in TiO2 and coke systems, Chem. Eng. J. 381 (2020) 122711. https://doi.org/10.1016/j.cej.2019.122711.

[77] C. Bu, B. Leckner, X. Chen, D. Pallarès, D. Liu, A. Gómez-Barea, Devolatilization of a single fuel particle in a fluidized bed under oxy-combustion conditions. Part A: Experimental results, Combust. Flame. 162 (2015) 797–808. https://doi.org/10.1016/j.combustflame.2014.08.015.

[78] W.-F. Chiang, H.-Y. Fang, C.-H. Wu, C.-J. Huang, C.-Y. Chang, Y.-M. Chang, C.-L. Chen, The Effect of Oxygen on the Kinetics of the Thermal Degradation for Rice Straw, J. Air Waste Manage. Assoc. 59 (2009) 148–154. https://doi.org/10.3155/1047-3289.59.2.148.

[79] Z. Xu, X. Xiao, P. Fang, L. Ye, J. Huang, H. Wu, Z. Tang, D. Chen, Comparison of Combustion and Pyrolysis Behavior of the Peanut Shells in Air and N2: Kinetics, Thermodynamics and Gas Emissions, Sustainability. 12 (2020) 464. https://doi.org/10.3390/su12020464.

[80] M. V. Gil, J. Riaza, L. Álvarez, C. Pevida, F. Rubiera, Biomass devolatilization at high temperature under N2 and CO2: Char morphology and reactivity, Energy. 91 (2015) 655–662. https://doi.org/10.1016/j.energy.2015.08.074.

[81] P. Fu, S. Hu, J. Xiang, L. Sun, S. Su, J. Wang, Evaluation of the porous structure development of chars from pyrolysis of rice straw: Effects of pyrolysis temperature and heating rate, J. Anal. Appl. Pyrolysis. 98 (2012) 177–183. https://doi.org/10.1016/j.jaap.2012.08.005.

[82] L.T. E. Biagini, F. Rossi, Effect of the Operating Conditions on the Devolatilization of Plastics, Eff. Oper. Cond. Devolatilization Plast. E. 2 (2002) 1–7.

[83] C. Di Blasi, C. Branca, I. Chimica, F. Ii, P. V Tecchio, Temperatures of Wood Particles in a Hot Sand Bed Fluidized by Nitrogen, (2003) 247–254.

[84] F. Miccio, S. Russo, N. Silvestri, Assessment of the devolatilization behavior of fuel pellets in fl uidized bed, Fuel Process. Technol. 115 (2013) 122–129. https://doi.org/10.1016/j.fuproc.2013.04.016.

[85] A.C. Rees, J.F. Davidson, J.S. Dennis, A.N. Hayhurst, The rise of buoyant fuel-particles in a slugging gas-fluidized combustor, Chem. Eng. Res. Des. 84 (2006) 319–327. https://doi.org/10.1205/cherd05043.

[86] A.S. Fung, F. Hamdullahpur, A gas and particle flow model in the freeboard of a fluidized bed based on bubble coalescence, Powder Technol. 74 (1993) 121–133. https://doi.org/10.1016/0032-5910(93)87004-8.

[87] R.J. de Korte, J.C. Schouten, C.M. van den Bleek, Controlling bubble coalescence in a fluidized-bed model using bubble injection, AIChE J. 47 (2001) 851–860. https://doi.org/10.1002/aic.690470409.

[88] J. Baron, E. Bulewicz, S. Kandefer, M. Pilawska, W. Zukowski, A. Hayhurst, The combustion of polymer pellets in a bubbling fluidised bed, Fuel. 85 (2006) 2494–2508.

https://doi.org/10.1016/j.fuel.2006.05.004.

[89] J.A.M. Kuipers, W. Prins, W.P.M. van Swaaij, Theorethical and experimental bubble formation at a single orifice in a two-dimensional gas-fluidized bed, Chem. Eng. Sci. 46 (1991) 2881–2894.

[90] J. F. Davidson and D. Harrison, Fluidised particles, Cambridge University Press, New York, 1963.

Highlights

- Devolatilization of highly-volatile feedstock in fluidized bed reactors is studied
- X-ray imaging provided qualitative and quantitative assessment of volatiles release
- Oxidizing conditions accelerate overall devolatilization time of feedstock particle
- Characterization of endogenous bubbles provided quantification of the lift effect
- Oxidizing/inert conditions do not affect endogenous bubbles properties